medRxiv preprint doi: https://doi.org/10.1101/2024.11.07.24316893; this version posted November 7, 2024. The copyright holder for this preprint (which was not certified by peer review) is the author/funder, who has granted medRxiv a license to display the preprint in perpetuity.
It is made available under a CC-BY-NC 4.0 International license .

Estimating behavioural relaxation induced by COVID-19 vaccines in the first months of their rollout

Yuhan Li[1], Nicolò Gozzi[2], Nicola Perra[1,3*]

[1] School of Mathematical Sciences, Queen Mary University of London, UK

[2] ISI Foundation, Turin, Italy

[3] The Alan Turing Institute, London, UK

[*] n.perra@qmul.ac.uk

Abstract

The initial rollout of COVID-19 vaccines has been challenged by logistical issues, limited availability of doses, scarce healthcare capacity, spotty acceptance, and variants of concern. Non-pharmaceutical interventions (NPIs) have been critical to support these phases. At the same time, the arrival of vaccines might have changed the risk assessment of some leading to a behavioural relaxation of NPIs. Several epidemic models have investigated the potential effects of this phenomenon on the COVID-19 pandemic, but they have not been validated against data. Recent empirical evidence, obtained via surveys, provides conflicting results on the matter. Hence, the extent behavioural relaxation induced by COVID-19 vaccines is still far from clear. Here, we aim to study this phenomenon in four regions. To this end, we implement five realistic epidemic models which include age structure, multiple virus strains, NPIs, and vaccinations. One of the models acts as a baseline, while the other four extend it and, building on the literature, include different behavioural relaxation mechanisms. First, we set the stage by calibrating the baseline model and running counterfactual scenarios to quantify the impact of vaccinations and NPIs. Our results confirm the critical role of both in reducing infection and mortality rates. Second, we calibrate the four behavioural models to real data and compare them to each other and to the baseline. While behavioural models offer a better fit of weekly deaths in all regions, this improvement is offset by their increased complexity in three locations. In the region where one of the behavioural model emerges as the most likely, our findings suggest that relaxation of NPIs led to a relative increase of deaths of more than 8%, highlighting the potential negative effect of this phenomenon. Overall, our work contributes to the retrospective validation of epidemic models developed amid the COVID-19 Pandemic.

NOTE: This preprint reports new research that has not been certified by peer review and should not be used to guide clinical practice.

medRxiv preprint doi: https://doi.org/10.1101/2024.11.07.24316893; this version posted November 7, 2024. The copyright holder for this preprint (which was not certified by peer review) is the author/funder, who has granted medRxiv a license to display the preprint in perpetuity.
It is made available under a CC-BY-NC 4.0 International license .

Introduction

In the Global North the first dose of COVID-19 vaccines was administered on December 8, 2020 [1]. Vaccines led to a significant reduction in mortality and transmission rates [2–4]. However, especially in the first months, vaccination efforts have encountered many challenges due to logistical issues, limited stockpiles and health care capacity, vaccine nationalism, and spotty vaccine acceptance [5]. A study from the United States, for instance, showed that counties with limited healthcare resources were also more likely to achieve lower COVID-19 vaccination rates [6]. Vaccine nationalism and socioeconomic inequities led to a concentration of doses in high-income countries [7, 8]. The insufficient vaccination coverage in many areas proved inadequate to prevent subsequent waves, thus leading to increased disease burden and to the implementation of additional interventions to curb the spread of SARS-CoV-2 [9, 10]. On a global scale, vaccine acceptance varied significantly across different regions, ranging from 13% in Iraq to 97% in Vietnam according to surveys conducted before the start of vaccine rollout [11]. Furthermore, the effectiveness of vaccines - especially in preventing transmission - was challenged by the emergence of new variants of concern (VOC) such as Alpha and Delta [12, 13].

While non-pharmaceutical interventions (NPIs) have been key to support vaccination efforts during these initial phases [10, 14, 15], their adoption is shaped by many factors such as perceived susceptibility, severity, barriers to actions, exposure to (mis)information, and peer-effects [16–22]. It is natural to wonder whether the arrival of COVID-19 vaccines impacted the adoption of NPIs. Indeed, the start of vaccinations might have lowered the perception of risk, at least in some groups of the population, which in turn might have led to a relaxation of NPIs. The potential effects of this phenomenon, which for simplicity we will refer to as behavioural relaxation, have been explored via epidemic models in realistic, yet theoretical, scenarios considering the first months of the vaccine rollout [23–26]. The results from these efforts suggest how behavioural relaxation could reduce the positive gains brought about by vaccines thus leading to higher disease burden. The empirical evidence does not provide a clear picture of the extent of behavioural relaxation. Indeed, some survey data report that vaccinated individuals had 1.31 times more social contacts [27] and increased mobility levels [28] with respect to non-vaccinated people. Other surveys conducted in Brazil, Italy, South Africa, and the United Kingdom, indicate that public transport usage increased by up to 10% after the rollout of first dose of vaccine [29]. However, the results from large, and repeated, cross-sectional surveys conducted in France provide limited support for a systematic behavioural relaxation, especially during the initial phases of the vaccine rollout [30].

In this context, we investigate the interplay between vaccinations and NPIs during the first months of the COVID-19 vaccine rollout in four regions: British Columbia (Canada), Lombardy (Italy), London (United Kingdom), and São Paulo (Brazil). These regions have been selected to sample different epidemiological, socioeconomic, and socio-demographic contexts. We set to quantify the extent of behavioural relaxations induced by the start of vaccination campaigns and estimate their potential impact

medRxiv preprint doi: https://doi.org/10.1101/2024.11.07.24316893; this version posted November 7, 2024. The copyright holder for this preprint (which was not certified by peer review) is the author/funder, who has granted medRxiv a license to display the preprint in perpetuity.
It is made available under a CC-BY-NC 4.0 International license .

on reported weekly deaths via epidemic models. Indeed, as mentioned above, the models published so far to capture such behavioural relaxation have not been validated against real data [23–26]. Besides, they have not been compared among them nor against a simpler baseline. By using the data collected and made available over the last years, we can address these gaps. To this end, we develop a series of stochastic compartmental epidemic models, integrating vaccinations, variants of concern, age-structure, NPIs as well as individuals' behavioural relaxation linked to vaccines. In particular, we consider a baseline model without behavioural relaxation mechanisms and four models that instead include them. In these, we introduce explicit compartments that account for non-compliant individuals who relaxed their protective behaviours as a result of the start of vaccinations. These models, which we will refer to as behavioural models, differ according to the mechanism used to describe the transitions in and out of non-compliant behavioural compartments. We calibrate and compare these models by using weekly deaths as epidemic target variable.

To set the stage, we first calibrate the baseline model to reported data and run two counterfactual scenarios to quantify the impact of vaccines and of NPIs on disease burden. Our results clearly confirm the crucial role played by both in reducing deaths and infections. Then, we calibrate and compare the other four models against each other and the baseline. We find that all models are able to reproduce the trajectories of the COVID-19 Pandemic in the four locations during the period considered. By studying the weighted mean absolute percentage errors (wMAPEs) we find that incorporating behavioural relaxation mechanisms improves the accuracy in all regions under study. However, when accounting for the increased complexity of these models via Akaike weights [31], we find the baseline to be the most likely model in three out of the four locations. Hence, by applying the Occam's razor principle, our results do not support the use of such behavioural relaxation mechanisms across all regions. To gather a better picture on the dynamics at play, we run another counterfactual scenario removing behavioural relaxation mechanisms from the four calibrated models. Interestingly, in the region where a behavioural models emerges as the most likely, this analysis suggests that the relaxation of NPIs led to a relative increase of deaths of more than 8%. Hence, our findings suggest how behavioural relaxation could be linked to a worsening of the Pandemic, at least in one of the locations studied. In the other regions our results do not exclude that some people did in fact relaxed their behaviours as result of the start of the vaccination campaign. They suggest that, if behavioural relaxation took place, it did not leave clear marks on confirmed weekly deaths raising the issue of identifiability of complex behavioural dynamics in epidemic models.

Overall, our results confirm the critical role of vaccines and NPIs in mitigating deaths and infections during the initial phases of the COVID-19 mass vaccination campaigns. At the same time, they provide an estimation of behavioural relaxation induced by vaccines in four regions. As we reflect on the COVID-19 Pandemic and prepare for the next one, studies that test and compare different models developed

medRxiv preprint doi: https://doi.org/10.1101/2024.11.07.24316893; this version posted November 7, 2024. The copyright holder for this preprint (which was not certified by peer review) is the author/funder, who has granted medRxiv a license to display the preprint in perpetuity.
It is made available under a CC-BY-NC 4.0 International license .

amid the emergency are of clear importance.

Results

We implement and compare five epidemic models. The first acts as a baseline. The others build on it and include different behavioural relaxation mechanisms. The four behavioural models combine and extend approaches from the literature [23, 24]. To explore different epidemiological, socioeconomic and socio-demographic contexts we consider four regions of the world: British Columbia (Canada), Lombardy (Italy), London (United Kingdom), and São Paulo (Brazil). All models are calibrated to confirmed weekly deaths via an Approximate Bayesian Computation-Sequential Monte Carlo (ABC-SMC) method [32]. While we provide a summary of the models in the next two sections, we refer the reader to the Material and Methods as well as section 1.1 in Supplementary Information for full details.

Baseline model

The baseline model (baseline) is a Susceptible-Latent-Infected-Recovered (SLIR) epidemic model integrating vaccinations, NPIs, age-structured contact matrices, multiple virus strains, and deaths. It constitutes the core upon which the other four models are built. We include age-stratified vaccinations by using real data [33–37]. For simplicity, we assume a single dose regiment and ignore the time required to develop full protection after inoculation. Furthermore, we assume that only Susceptible individuals are eligible for vaccination. We estimate the impact of NPIs on social contacts using mobility data from the COVID-19 Community Mobility Report published by Google LLC [38] and the Oxford Coronavirus Government Response Tracker (OxCGRT) [39]. This data is used to modulate the contact matrices as function of time. We also consider the spread of a second virus strain. According to virological surveillance data, during the period under consideration, the Alpha variant emerged and replaced the ancestral type in British Columbia and Lombardy, while Delta replaced the Gamma VOC in São Paulo. London, during the time interval under investigation, faced primarily a wave dominated by the Alpha VOC [40–42]. In our models, we assume Alpha and Delta to have higher transmissibility [43, 44], immune escape potential [43, 45, 46], and shorter latent period with respect to previously circulating strains [47–51]. We refer the reader to the Materials and Methods for more details.

Behavioural relaxation models

Building on the baseline and the literature, we explore four different behavioural relaxation models. To this end, we extend the compartmental structure of the baseline by introducing non-compliant (NC) compartments to account for susceptible individuals (both vaccinated or not) who relax their COVID-19 safe behaviours as result of the vaccine rollout. Individuals in the NC compartments have a proba-

medRxiv preprint doi: https://doi.org/10.1101/2024.11.07.24316893; this version posted November 7, 2024. The copyright holder for this preprint (which was not certified by peer review) is the author/funder, who has granted medRxiv a license to display the preprint in perpetuity.
It is made available under a CC-BY-NC 4.0 International license .

bility of infection that is r ($r > 1$) times higher than that of compliant individuals [23, 24, 27]. The four behavioural models differ for the mechanisms regulating the transitions from and to compliance. Following Ref. [23] in the first (model 1) and second (model 2) behavioural model we assume that all susceptible individuals (vaccinated or not) might enter/leave the NC compartments. In detail, in the first model the transition rates between compliance and non-compliance are constant and equal to α and γ respectively. In the second behavioural model, susceptible individuals enter/leave the NC compartment at varying rates. The transition rate to non-compliant behaviour is set as a function of the fraction of vaccinated individuals and a parameter α. The reverse transition rate is instead set as a function of the number of reported daily deaths per $100,000$ and a parameter γ. Indeed, daily deaths have been used by media to characterize the status of the Pandemic and are known to have influenced individuals' adherence NPIs [16]. Following Ref. [24] the third (model 3) and fourth (model 4) behavioural models are respectively analogous to model 1 and model 2. However, in these two only vaccinated individuals might transition to non-compliant compartments.

Vaccines rollout, epidemic progression and NPIs in the four regions under study

The rollout of COVID-19 vaccines is a key part of our work. Hence, we start by providing some information about the initial phases of vaccinations in the four regions under study. In Fig. 1-A, we show the 7-day moving average of the fraction of daily newly vaccinated individuals across all age groups (shaded areas) and in the 70+ age group (solid lines) from the start of the vaccination rollout until the end date of the period under consideration. COVID-19 vaccination campaigns started on 2020/12/19 in British Columbia, 2020/12/08 in London, 2020/12/27 in Lombardy, and 2021/01/18 in São Paulo [33–37]. In all locations, we observe a peak in the first month during which the initial doses were mainly administered to healthcare workers and fragile individuals. A similar behaviour can be seen for the 70+ age group. Moreover, the vaccine rates of this group show a second peak earlier with respect to the overall vaccination rates in the four regions, reflecting the priority given to the elderly population. Additionally, we observe how the vaccination rate in London was concentrated during the second to the fifth month since the rollout started. In British Columbia and Lombardy instead, vaccination started on a wide scale (i.e., beyond the prioritization of fragile individuals and healthcare workers) from the third month of the rollout, and even later in São Paulo (from the fourth month).

To better understand the epidemic contexts in the periods under examination, next we discuss the evolution of the Pandemic and of NPIs in the four regions. In Fig. 1-B we show the confirmed deaths per $100,000$ (solid lines). We can observe differences in the timing, shape, and intensity of the Pandemic across the four regions. Indeed, within the time horizon of interest, British Columbia and London experienced a single peak concentrated around the end of 2020. The peak in London was particularly

medRxiv preprint doi: https://doi.org/10.1101/2024.11.07.24316893; this version posted November 7, 2024. The copyright holder for this preprint (which was not certified by peer review) is the author/funder, who has granted medRxiv a license to display the preprint in perpetuity.
It is made available under a CC-BY-NC 4.0 International license .

intense and fuelled by the spread of the Alpha VOC which was initially detected there and traced back to a set of transmission chains that occurred in September 2020 [52]. In British Columbia, instead, the peak was more than five times less intense and followed by a slower decrease with fluctuations due to the Alpha variant replacing the wild type [53]. In Lombardy, we observe an intense peak (comparable to London) right before the end of the year and a second, less pronounced, peak in early April mainly due to the lifting of some of the NPIs and the spreading of Alpha [14]. Also in São Paulo we observe two intense peaks, which however are much closer both in terms of intensity and timing. Genomic data in this region suggests that the two peaks were driven by the rapid spread of the Gamma VOC first followed by the arrival and spread of the Delta VOC [42, 54, 55]. We note how the first of these two peaks take place in April, hence months later the main peak in the other three areas.

In Fig. 1-B we also show the effects of NPIs on contacts estimated from the COVID-19 Community Mobility Report released by Google [38] and the Oxford Coronavirus Government Response Tracker (OxCGRT) [39]. We use this data to compute the contact levels during the Pandemic with respect to a pre-Pandemic baseline. Indeed, this data has been often used as a proxy of NPIs adoption, especially during the first two years of the Pandemic [16]. We refer the reader to the Materials and Methods for details. The plot suggests that, among the regions considered, individuals in London adopted the strictest NPIs. This is likely due to the emergence and rapid spread of the Alpha VOC that resulted in strong social distancing policies. These measures led to a significant reduction in contacts ranging from 10% to 50% with respect to the pre-pandemic contact levels. A similar trend, though not as strong, is observed in Lombardy where contacts rapidly dropped as the 2020 winter season progressed. In British Columbia, despite a visible drop at the end of 2020, we observe a slow increasing trend centred around 50% with respect to the pre-pandemic baseline. Similar trends are observed in São Paulo where, however, we can observe a much steeper increase in contacts, back to, and even larger than, the pre-pandemic baseline in the second half of 2021.

Baseline calibration

In Fig. 1-C, we show the weekly deaths as reported by official surveillance and as estimated by the baseline epidemic model in the four regions considered. In the figure, we plot medians along with 90% confidence intervals (CI) computed considering 1000 stochastic trajectories sampled from the empirical joint posterior distribution estimated via the ABC-SMC calibration (see Materials and Methods for details). We highlight the start of the vaccination campaign in each location with vertical solid lines. To account for local differences in the epidemic trajectory, the starting point of our simulations is left as a free, calibrated, parameter (see Materials and Methods for more details). Furthermore, the simulation horizons in the four regions are set to capture the local epidemic wave(s) in the first months of the vaccine rollout. More precisely, we run simulations until 2021/07/04 in British Columbia, London, and

medRxiv preprint doi: https://doi.org/10.1101/2024.11.07.24316893; this version posted November 7, 2024. The copyright holder for this preprint (which was not certified by peer review) is the author/funder, who has granted medRxiv a license to display the preprint in perpetuity.
It is made available under a CC-BY-NC 4.0 International license .

Lombardy. In case of São Paulo we run until 2021/10/03 to capture the late waves of infection experienced there with respect to the other regions. Interestingly, most reported data points fall within the 90% CI of the calibrated baseline, which suggests the effectiveness of the model in fitting the unfolding of the Pandemic in the four locations. The analysis of the posterior distributions of free parameters, shown in section 5.2 of the Supplementary Information, indicates London as the region with the highest basic reproductive number R_0. This is likely due the dominance of the Alpha VOC in London at the start of our simulation window.

Estimating the impact of vaccines and NPIs via counterfactual scenarios

To estimate the impact of vaccines we run a counterfactual scenario where they are removed from the baseline model. To this end, we first calibrate the model in the four locations. Then, we run matched simulations where we remove vaccinations. Hence, we quantify the effect of vaccines by computing the fraction of total deaths avoided by vaccines with respect to the deaths observed in an equivalent model without vaccines. This fraction, describing the relative deaths difference (RDD) (see more details in Materials and Methods), is shown Fig. 2-A. The median values of RDD are greater than zero highlighting the clear positive effects of vaccinations. In particular, we find an RDD of 3.85% (90% CI: [−0.22%,9.39%]) in British Columbia, 12.77% ([9.11%,16.13%]) in Lombardy, 7.65% ([1.57%,18.9%]) in London, and 48.22% ([42.05%,53.75%]) in São Paulo. The difference in RDD across the four regions is possibly due to several factors including timing and coverage of vaccines, local epidemiological context (e.g., VOC circulating), and NPIs in place. Notably, São Paulo, which exhibits the highest RDD, achieved also the highest vaccine coverage (78% of the population) by the end date of the simulation window. This is significantly larger than the coverage in British Columbia (69%), Lombardy (63%), and London (61%). Notably, the median value of RDD in São Paulo corresponds to more than $60K$ additional deaths averted (see section 3.5 in Supplementary Information). Though British Columbia has marginally higher vaccine coverage compared to Lombardy and London, its RDD is however the lowest (with some negative outliers due to stochastic fluctuations). This discrepancy can be explained by the relatively lower and slower epidemic progression in this region. As mentioned, this location experienced, at the peak, a burden of the disease about five times lower than the other three. Consistently, the estimated reproductive number is also the smallest. The RDD values in this region are reflective of a very small absolute difference between the two scenarios (about 60 deaths as shown in section 3.5 in Supplementary Information). Such small values are subject to stochastic effects and should be interpreted carefully. The RDDs in Lombardy and London are similar, with London showing a slightly lower value compared to Lombardy. In London the early 2021 wave was fuelled by the Alpha VOC which was more transmissible and able to reduce the vaccines' protection from infection. Besides, the time window for computing RDD is slightly longer in Lombardy than London.

medRxiv preprint doi: https://doi.org/10.1101/2024.11.07.24316893; this version posted November 7, 2024. The copyright holder for this preprint (which was not certified by peer review) is the author/funder, who has granted medRxiv a license to display the preprint in perpetuity.
It is made available under a CC-BY-NC 4.0 International license .

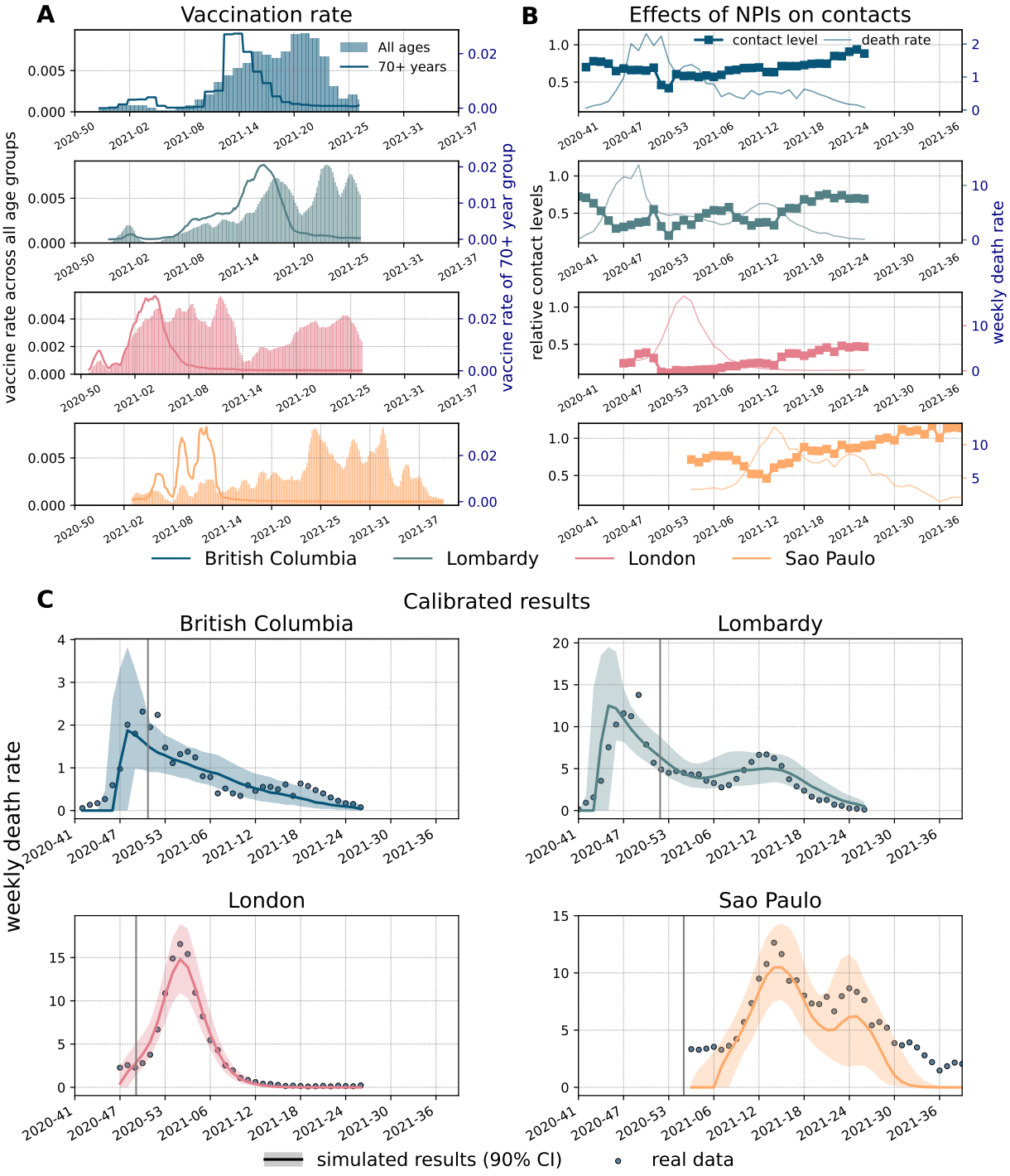

Fig 1. Weekly deaths, vaccinations, contacts reduction, and calibration of baseline model. A) Fraction of daily newly vaccinated individuals across all age groups (shaded areas) and within the 70+ age-group (solid lines) in the four regions from up to down: British Columbia, Lombardy, London, and São Paulo. B) Contact levels during the Pandemic with respect to a pre-pandemic baseline. C) Reported data describing weekly deaths per 100, 000 (dots) and the results from the calibrated baseline model (solid lines representing the medians, shaded areas the 90% confidence intervals). The grey vertical lines mark the start of vaccinations in different regions.

medRxiv preprint doi: https://doi.org/10.1101/2024.11.07.24316893; this version posted November 7, 2024. The copyright holder for this preprint (which was not certified by peer review) is the author/funder, who has granted medRxiv a license to display the preprint in perpetuity.
It is made available under a CC-BY-NC 4.0 International license .

Analogously, we compute relative difference of infections (RDI), defined as the fraction of total infections avoided by vaccines with respect to the infections observed in an equivalent model without vaccines (see Section 3.3 in Supplementary Information for details). In general, the RDIs are lower compared to RDDs across the regions as vaccines are more effective in preventing severe outcomes rather than infection. The RDIs show a similar pattern to that observed for RDDs across the four regions, except for São Paulo. The median of RDIs is only 9% while it is 48% for RDDs. This is likely due to São Paulo experiencing distinct viral strains, specifically the Gamma and Delta variants, which significantly reduces vaccine efficacy against infection compared to the other regions that instead saw the circulation of the wild type and the Alpha variant [43].

Furthermore, to investigate when the vaccination began to have macroscopic effects on deaths, we compute when, in the simulations, weekly deaths with and without vaccination begin to diverge by more than 1%. We found that, in median terms, the vaccination effects started 8 weeks after the first vaccination in London. This is earlier than that in British Columbia, Lombardy, and São Paulo, in which the vaccine effects started, respectively, 12, 10, and 10 weeks after the first dose. The difference is likely due to the faster and earlier vaccine rollout in London with respect to the other regions. We refer the reader to section 3.1 in the Supplementary Information for further details on this analysis.

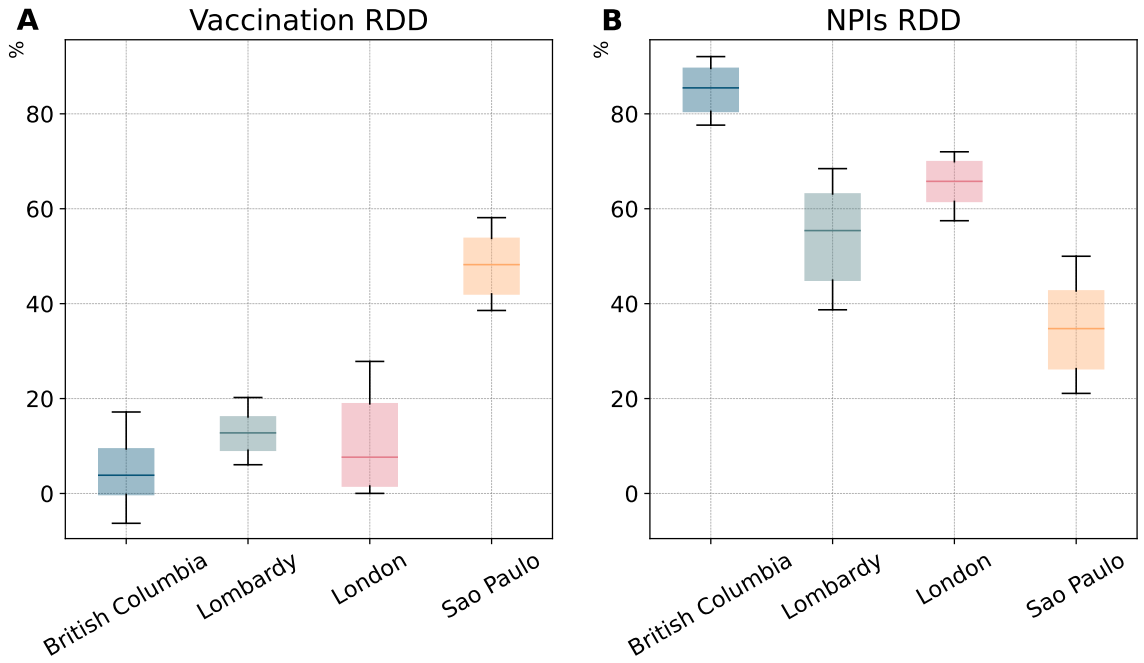

Fig 2. Impact of vaccines and non-pharmaceutical interventions on COVID-19 deaths (baseline model). A) Fraction of total COVID-19 deaths averted by vaccinations with respect to a model without vaccinations. B) Fraction of total COVID-19 deaths averted by the implementation of NPIs with respect to a model without NPIs. The boxplots in both panels show the results considering 1000 sampled stochastic trajectories in each region. These estimates are obtained considering the baseline model.

To investigate the effects of NPIs on the progression of the Pandemic, we run a counterfactual scenario where we remove the impact of NPIs on contacts, while maintaining vaccinations. By comparing the

medRxiv preprint doi: https://doi.org/10.1101/2024.11.07.24316893; this version posted November 7, 2024. The copyright holder for this preprint (which was not certified by peer review) is the author/funder, who has granted medRxiv a license to display the preprint in perpetuity.
It is made available under a CC-BY-NC 4.0 International license .

trajectory of deaths with/without contacts modulation induced by NPIs, we found that without NPIs we would have experienced a larger number of deaths across all regions considered. Specifically, our results show that removing NPIs would have resulted in a much higher peak of weekly deaths, 5.5 (90% CI: [2.8, 11.3]) times higher in British Columbia, 2.8 ([1.8, 4.6]) times higher in Lombardy, 6.1 ([5.0, 7.6]) times higher in London, and 4.6 [3.8, 5.7] times higher in São Paulo compared to the estimates of the model considering NPIs. The absence of NPIs would have led to a 3 weeks earlier peak of weekly deaths in London and 2 weeks São Paulo (see Section 3.2 in the Supplementary Information). Furthermore, we quantify the effect of NPIs by computing the fraction of total deaths avoided by NPIs with respect to the deaths observed in an equivalent simulation without NPIs (denoted by RDD as above). As shown in Fig 2-B we find that 85.47% (90% CI: [80.51%, 89.58%]) deaths have been avoided due to NPIs in British Columbia, 55.40% ([44.95%, 63.11%]) in Lombardy, 65.77% ([61.56%, 69.91%]) in London, and 34.74% ([26.30%, 42.68%]) in São Paulo. Not surprisingly, the RDD of the four regions are strongly correlated with their contact reduction with an exception in British Columbia. Specifically, British Columbia shows the highest RDD despite not featuring the strongest reduction in contacts. As noted above, the peak height of weekly deaths in British Columbia is more than five time smaller than the other regions. Hence, the NPIs in place, and their adoption, successfully managed to reduce the burden of the disease more than in the other locations. Thus, relatively speaking, without NPIs the picture in British Columbia would have been drastically different. The RDD of London is the second largest due to the strict NPIs implemented during the observed period, imposed by the emergence and spreading of the Alpha VOC in September 2020. In contrast, São Paulo exhibits the lowest RDD, due to the relative low reduction in contacts induced by NPIs.

Analogously, we compute the fraction of total infections avoided by NPIs with respect to the infections estimated by an equivalent model without NPIs (denoted by RDI as mentioned above, see details in Section 3.3 in the Supplementary Information). The results of RDIs of the four regions are consistent with the results of RDD, except for London that shows lower RDIs than Lombardy. This may be explained considering that Lombardy has a larger population of elderly with respect to London (see section 3.3 in Supplementary Information for more details).

Comparing panels A and B in Fig. 2, we see that, in the first months of the vaccine rollout, NPIs averted more deaths than vaccinations underscoring the crucial role of NPIs in supporting the initial critical phases of mass vaccine campaigns that, as discussed, struggled with colossal challenges.

Estimating the extent of behavioural relaxation induced by vaccines

Building on the baseline and the literature, we developed four behavioural models (models 1-4) where we incorporate behavioural relaxation mechanisms potentially induced by vaccines. In Fig. 3, we show the calibrated results of all the models (including the baseline) by presenting the medians and the 90%

medRxiv preprint doi: https://doi.org/10.1101/2024.11.07.24316893; this version posted November 7, 2024. The copyright holder for this preprint (which was not certified by peer review) is the author/funder, who has granted medRxiv a license to display the preprint in perpetuity.
It is made available under a CC-BY-NC 4.0 International license .

confidence intervals of weekly deaths. The calibrated curves are all consistent with reported epidemiological data. The differences between the five models appear minimal to a visual inspection. To better investigate the nuances of these models, we use weighted mean absolute percentage errors (wMAPEs) and Akaike Information Criteria (AIC) scores [56]. The wMAPE measures the difference between the median outcomes of our models and reported data, while AIC scores assess the performance of models by trading off their complexity and the goodness of fit. Based on the AIC scores, we further calculate the AIC weight of each model for a more intuitive interpretation [31]. These weights can be interpreted as the probability that a model, among those considered, is the most likely given the empirical data [31]. While we only display AIC weights in the main text, we refer the reader to the Supporting Information for the AIC scores.

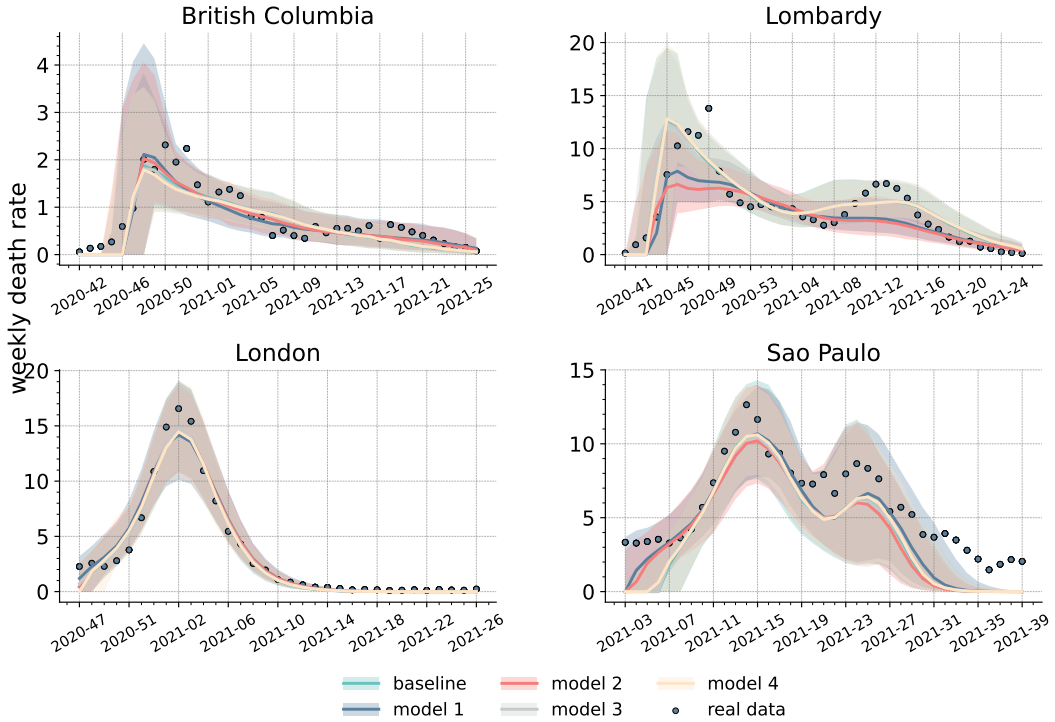

Fig 3. Comparison of behavioural and baseline models. Calibrated weekly death trajectories (weekly deaths per 100,000) for the baseline and four behavioural models across the four regions. Solid lines indicate the medians, while the shaded areas the 90% confidence intervals. Reported weekly deaths are denoted by blue dots.

The wMAPEs of the five models are shown in Table 1. Interestingly, behavioural models outperform the baseline in the four regions. The best model results in an improvement of 9.7% in WMAPEs in British Columbia, 14.7% in Lombardy, 2.5% in London, and 26.7% in São Paulo compared to the baseline. In more detail, model 1 results the best in Lombardy, model 2 in British Columbia and São Paolo, and model 3 in London. Hence, in three out of four locations behavioural models that extend the possibility of non-compliance to NPIs to all susceptible, independently from their vaccination status (i.e., model 1 and 2), better reproduce reported data.

The picture changes, when we account for the complexity of the models. Indeed, according to AIC

medRxiv preprint doi: https://doi.org/10.1101/2024.11.07.24316893; this version posted November 7, 2024. The copyright holder for this preprint (which was not certified by peer review) is the author/funder, who has granted medRxiv a license to display the preprint in perpetuity.
It is made available under a CC-BY-NC 4.0 International license .

Table 1. wMAPEs between estimated models' medians and reported weekly deaths. Lowest wMAPE in each location is highlighted in bold.

	baseline	model 1	model 2	model 3	model 4
British Columbia	0.259	0.235	**0.234**	0.258	0.258
Lombardy	0.266	**0.227**	0.260	0.259	0.243
London	0.130	0.142	0.127	**0.125**	0.142
São Paulo	0.290	0.232	**0.213**	0.217	0.221

weights, the baseline is the most likely model in three regions (see Table 9). In São Paulo, instead, model 2 (followed by the baseline) is the most likely. These results show that, although behavioural mechanisms improve the goodness of fit, they come at the cost of an increased complexity that does not offset the gains in fitting the epidemic curves of three regions. Following Occam's razor principle, we can conclude that the inclusion of behavioural relaxation mechanisms is not fully justified, at least when looking at weekly deaths in the three out of four regions studied. A simpler model, that does not explicitly account for this phenomenon, appears well suited to reproduce the unfolding the epidemic indicator in the majority of locations. Nevertheless, it is important to stress how our results do provide evidence for behavioural relaxation in one of the regions. Including these effects not only decreases the wMAPE by more than 20%, but the gains in the fit cannot be explained just by the larger number of parameters.

Table 2. AIC weights computed on estimated models' medians and reported weekly deaths. Highest AIC weight in each location is highlighted in bold.

	baseline	model 1	model 2	model 3	model 4
British Columbia	**0.83**	0.05	0.05	0.04	0.04
Lombardy	**0.91**	0.00	0.05	0.03	0.01
London	**0.84**	0.02	0.07	0.04	0.02
São Paulo	0.37	0.00	**0.52**	0.05	0.05

In order to gather a better understanding of the dynamics at play, and to isolate the potential effects of behavioural relaxation on deaths, we run another counterfactual analysis removing the relaxation mechanisms in the four behavioural models. In doing so, we compute the relative deaths difference (RDD) between the models with/without behavioural relaxation. As shown in Fig. 4 and in Table 5, the median RDD values are below zero in the large majority of cases, indicating that removing behavioural relaxation generally results in fewer deaths. The results show that models 1 and 2 lead to a larger difference in deaths (especially in Lombardy and São Paulo) compared to models 3 and 4 which restrict behavioural relaxation to vaccinated individuals only. Not surprisingly, the impact of non-compliance extended to the whole population is higher. We note how in São Paulo, where model 2 emerges as the most likely, the effects of behavioural relaxation is quantified in more than 8% additional deaths. Hence, our results highlight the negative impact of this phenomenon on COVID-19 death toll.

Finally, we compute the relative infection difference (RDI) (shown in section 3.4 in Supplementary Information), which shows consistent results with those of RDDs.

medRxiv preprint doi: https://doi.org/10.1101/2024.11.07.24316893; this version posted November 7, 2024. The copyright holder for this preprint (which was not certified by peer review) is the author/funder, who has granted medRxiv a license to display the preprint in perpetuity.
It is made available under a CC-BY-NC 4.0 International license .

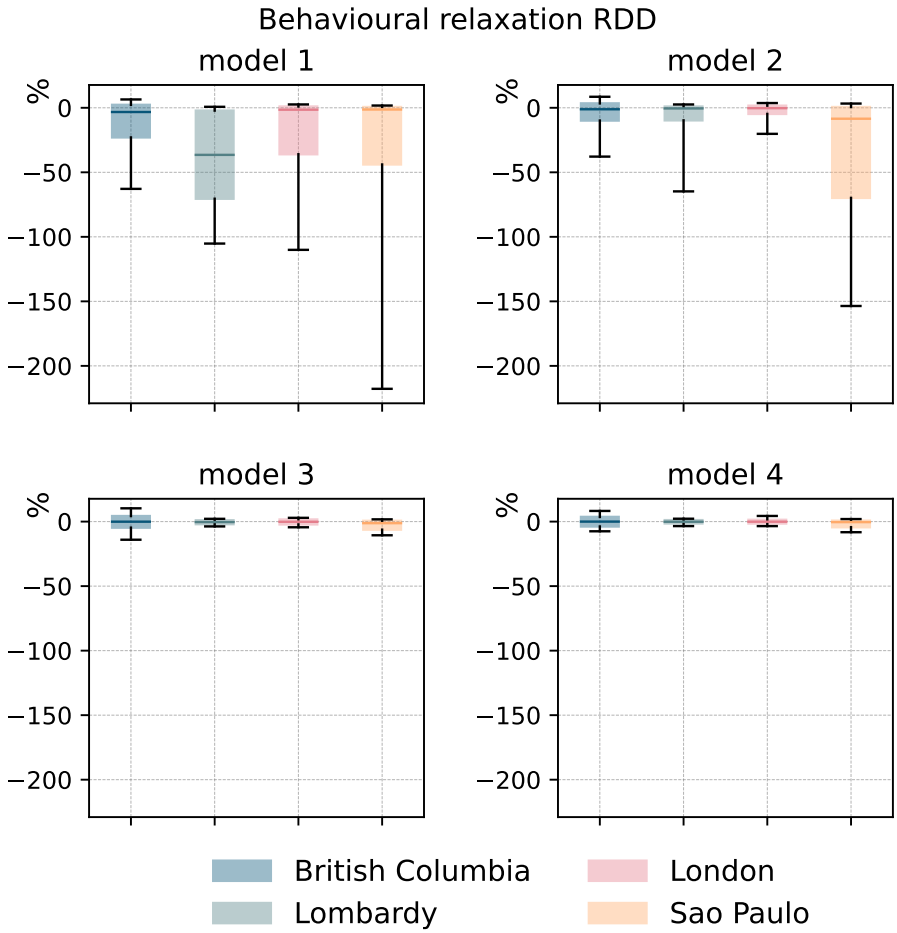

Fig 4. The impact of behavioural relaxation on COVID-19 deaths (behavioural models). For the four behavioural models and the four regions we plot the distribution of RDD (i.e., relative deaths difference). Each boxplot is built considering 1000 stochastic simulations.

Discussion

In this paper, we aimed to find signs, and to quantify the extent of behavioural relaxation possibly induced by vaccines during the initial phase of the COVID-19 vaccine rollout. To this end, we developed a series of stochastic epidemic compartmental models integrating age-structure, vaccinations, NPIs, variants of concern, and deaths. We used a baseline model, without any behavioural relaxation mechanism, as a reference, and on top of this, we developed four behavioural models that extended previous work to account for individual behaviours in response to vaccination and the epidemic [21–26]. We tested these models considering weekly deaths in four regions: British Columbia (Canada), Lombardy (Italy), London

Table 3. Relative deaths difference estimated in counterfactual scenarios without relaxation in behavioral models. Medians and 90% confidence intervals are reported. Numbers indicate percentages.

RDD (%)	model 1	model 2	model 3	model 4
British Columbia	-3.27 [-22.95,2.28]	-1.14 [-9.89,3.41]	-0.06 [-4.69,4.29]	0.0 [-3.79,3.63]
Lombardy	-36.48 [-70.47,-2.19]	-0.49 [-9.74,0.95]	-0.36 [-1.99,1.03]	-0.1 [-1.41,1.14]
London	-1.48 [-35.99,0.99]	-0.29 [-4.75,1.62]	-0.14 [-2.18,1.63]	-0.07 [-1.48,1.38]
São Paulo	-1.33 [-43.91,0.6]	-8.48 [-69.82,0.59]	-1.22 [-6.23,0.61]	-0.4 [-4.37,0.73]

medRxiv preprint doi: https://doi.org/10.1101/2024.11.07.24316893; this version posted November 7, 2024. The copyright holder for this preprint (which was not certified by peer review) is the author/funder, who has granted medRxiv a license to display the preprint in perpetuity.
It is made available under a CC-BY-NC 4.0 International license .

(United Kingdom), and São Paulo (Brazil). These locations sample different epidemic, socioeconomic and socio-demographic contexts. We first calibrated the baseline model to reported data and studied two counterfactual scenarios to quantify the impact of vaccines and NPIs on COVID-19 deaths and infections. Our results confirmed that both significantly reduced mortality and infections. Furthermore, they highlighted the critical role of NPIs in supporting the challenging initial phases of vaccinations. We then calibrated the four behavioural models and compared them considering both their goodness of fit and complexity. Behavioural models estimates are closer to real data than the baseline. However, behavioural mechanisms increase models' complexity which is not offset by the benefits of improved fits in three out of the four regions. This suggests that additional mechanisms of behavioural relaxation linked to vaccination may not be evident across all regions. Finally, we isolated the impact of behavioural relaxation with another counterfactual scenario finding that adding these mechanisms might lead to significant variations on the target variable (i.e., weekly deaths) especially when the behavioural relaxation is not restricted to the vaccinated population. Furthermore, we find that in São Paulo, the region where one of the behavioural model emerges as the most likely, behavioural relaxation might have led to an additional 8% deaths. Notably, this corresponds to about 5000 deaths. In line with results from some surveys [27–29] and theoretical modelling efforts [23, 24], our findings highlight and quantify the negative impact of relaxation of NPIs in the initial critical phases of a mass vaccination campaign.

At the same time, our results indicate that behavioural relaxation did not leave clear marks in the other three regions. This finding, in line with surveys conducted in France [30], might be interpreted as a lack of support for systematic behavioural relaxation induced by COVID-19 vaccines in those locations. However, our findings cannot exclude that, in fact, behavioural relaxation took place also in these regions. Indeed, the lack of clear signs on weekly deaths is compatible with at least three other hypotheses. First, behavioural relaxation might have taken place but not to the levels needed to affect deaths at a macroscopic scale. Second, behavioural relaxation might have impacted deaths, but these effects could be accounted for by simpler models that do not explicitly consider additional mechanisms. In our settings, the effects of behavioural relaxation might be fully captured by the modulation of contacts induced by NPIs. This interpretation raises the important issue of identifiability of complex behavioural mechanisms in epidemic models when using a single macroscopic indicator as target. Somehow in the middle between the previous two we have a third hypothesis: signs of behavioural relaxation might be clearer in other indicators. For example, given the strong dependence of COVID-19 mortality on age [57], behavioural relaxation might have primarily affected infections, especially among the young, active population, rather than deaths. Unfortunately, real data on confirmed cases has been shown to be a poor indicator and a very hard signal to fit due to under-reporting and variations in testing policies among other factors [58]. Clearly more work, including a wider range of indicators and data, is need to evaluate these hypotheses and to reconcile the contrasting results from past surveys.

medRxiv preprint doi: https://doi.org/10.1101/2024.11.07.24316893; this version posted November 7, 2024. The copyright holder for this preprint (which was not certified by peer review) is the author/funder, who has granted medRxiv a license to display the preprint in perpetuity.
It is made available under a CC-BY-NC 4.0 International license .

Our work comes with limitations. First, the epidemiological and vaccination data are sourced from different datasets. Although the data has been obtained from official sources, the granularity provided is not homogeneous. Second, we considered a simplified vaccination protocol assuming that only susceptible individuals can get vaccinated and a single dose regiment. These assumptions have been made to simplify the model structure. Third, we used regional-level data regarding school closures for British Columbia, London, and São Paulo but country-level data for Lombardy, due to the lack of specific regional data. Moreover, there is lack of available data to parametrize the rates regulating behavioural relaxation. As a consequence, we had to calibrate the behavioural parameters within some rather arbitrary ranges. Fourth, though we accounted for a higher transmission rate, shorter latent period, and decreased vaccine efficacy for the second variant, we used the same infection fatality rate (IFR) across all strains and regions. Finally, our model does not account for socioeconomic nor socio-demographic differences in vaccines uptake nor in adoption of NPIs [59, 60].

Overall, our work highlights the critical importance of both NPIs and vaccines in curbing COVID-19 deaths and infections during the initial months of COVID-19 vaccination campaigns. Our findings pave the way for further research to refine the proposed models and deepen our understanding of the interaction between individual protective behaviour and vaccinations in a broader context.

Materials and Methods

Baseline model

As baseline we adopt a stochastic age-stratified epidemic compartmental model that integrates vaccination, NPIs, and the emergence/spread of a second variant based on a Susceptible-Latent-Infected-Recovered (SLIR) compartmentalization extended to account for deaths. Individuals are grouped into 16 age brackets with a five-year interval (except for the last group which is 75+). We use age-stratified Infection Fatality rates (IFR) from Ref. [57] and age-stratified contact matrices from Ref. [61]. The natural history of the disease is modelled as follow. By interacting with the Infected (I), Susceptible (S) individuals transition to the latent stage (L compartment) where they are infected but not yet infectious. We assume a force of infection (i.e., the rate at which Susceptible get infected) function of age, transmissibility of each strain, contact matrices, and NPIs (see below for details). Individuals stay in L for an average of ϵ^{-1} time steps. After, they become infectious transitioning to the I compartment. After the infectious period μ^{-1}, infected individuals either recover with probability $(1 - IFR_k)$ (transitioning to the R compartment) or die from the disease with probability IFR_k (transitioning to the D compartment), where k denotes the age-group. We also consider a delay of Δ time steps in reporting deaths. Therefore, individuals are moved to the D^o compartment from D after Δ time steps.

medRxiv preprint doi: https://doi.org/10.1101/2024.11.07.24316893; this version posted November 7, 2024. The copyright holder for this preprint (which was not certified by peer review) is the author/funder, who has granted medRxiv a license to display the preprint in perpetuity.
It is made available under a CC-BY-NC 4.0 International license .

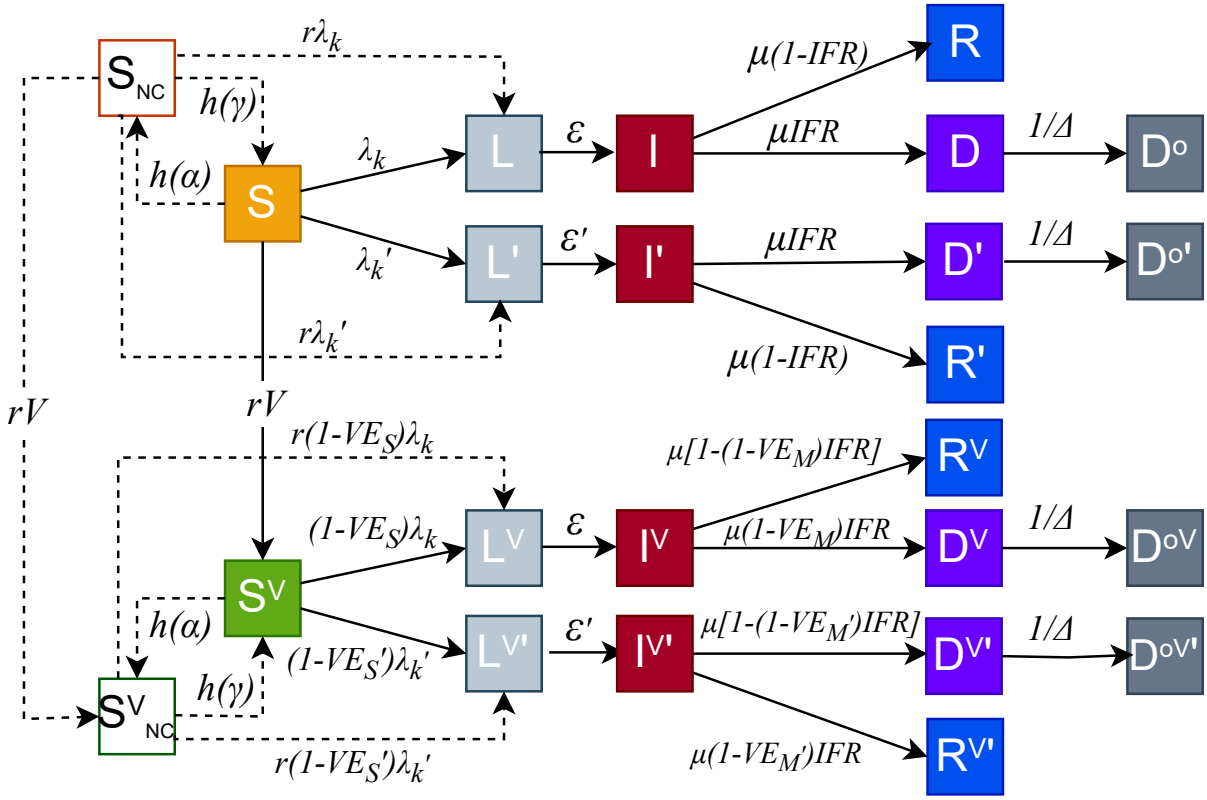

Fig 5. Epidemic compartment structure. All compartments connected by solid lines constitutes the baseline model. This model includes susceptible (S), latent (L), infected (I), recovered (R), and dead (D, D^o) compartments. The top row represents non-vaccinated compartments, whereas the bottom row represents vaccinated compartments. Individuals in the S compartment get vaccinated according to real vaccine rates (rV) and then transition to the S^V compartment. To account for the emergence of a second variant, we double the compartments creating L', I', R', D', and $D^{o'}$. This is done also for the vaccinated compartments that become $L^{V'}$, $I^{V'}$, $R^{V'}$, $D^{V'}$, $D^{Vo'}$. Behavioural models include susceptible non-compliant compartments (S_{NC}, S^V_{NC}) connected by dotted lines, where individuals have r times higher probability of getting infected with respect to susceptible compliant individuals (S and S^V). In models 1 and 2, we include S_{NC} and S^V_{NC}, whereas in models 3 and 4 we include only S^V_{NC}.

medRxiv preprint doi: https://doi.org/10.1101/2024.11.07.24316893; this version posted November 7, 2024. The copyright holder for this preprint (which was not certified by peer review) is the author/funder, who has granted medRxiv a license to display the preprint in perpetuity.
It is made available under a CC-BY-NC 4.0 International license .

Modelling vaccinations

We incorporate vaccinations into our models by doubling all the compartments to include vaccinated individuals at any stage of the disease. We assume that only susceptible individuals can receive the vaccine. Additionally, to simplify the model, we disregard the time interval between the first and second dose. Consequently, we assume that individuals acquire full protection right after the first inoculation. We use real data to capture the unfolding of the vaccination campaigns in the four regions [33–37]. Notably, vaccine data are recorded weekly in official statistics in British Columbia while the other three regions report vaccine data daily. Thus, in British Columbia, we convert the weekly doses into daily by splitting them homogeneously in each week day. Vaccines protect individuals in two ways: by lowering the risk of infection, and by reducing the risk of death in case of breakthrough infection. In practice, for vaccinated individuals the force of infection is multiplied by a factor $1 - VE_S$, where VE_S denotes the vaccine's efficacy against infection. If a vaccinated individual becomes infected, the IFR is further reduced by a factor $1 - VE_M$, where VE_M represents the vaccine's efficacy against death. Therefore, the overall vaccine efficacy for a susceptible individual, against death, is $VE = 1-(1-VE_S)(1-VE_M)$.

Modelling the impact of NPIs on contacts.

In age-structured epidemic models, contact matrices $\mathbf{C}$ stratify interactions among age groups [61]. Contact matrices might be further stratified by the context (i.e., location) where contacts take place: home, school, workplace, and general community settings [62]. Here, we consider both dimensions and express the overall contact matrix as the sum of the contact matrices of each context:

$$\mathbf{C} = \mathbf{C}_{home} + \mathbf{C}_{work} + \mathbf{C}_{school} + \mathbf{C}_{others} \tag{1}$$

To estimate the variations in contact rates due to NPIs, we use mobility data from the COVID-19 Community Mobility Report released by Google [38] and the Oxford Coronavirus Government Response Tracker (OxCGRT) [39]. In particular, we use this data to adjust the contact matrix as follows:

$$\mathbf{C}' = \mathbf{C}_{home} + w_{work}\mathbf{C}_{work} + w_{school}\mathbf{C}_{school} + w_{others}\mathbf{C}_{others} \tag{2}$$

where $\mathbf{C}'$ is the adjusted contact matrix, w_{work} and w_{others} are computed as $(1 - x/100)^2$, where x is the percentage of change in mobility with respect to a pre-Pandemic baseline measured by Google [38]. We use a square form as the number of contacts in a location scales proportional to the square of people visiting that location [10, 14]. In particular, w_{work} is computed considering the field related to workplaces of the Google Mobility Report, while w_{others} considering an average of the fields related to retail and recreation and transit stations. Furthermore, w_{school} is computed as $(3 - school)/3$, where $school$ is an

medRxiv preprint doi: https://doi.org/10.1101/2024.11.07.24316893; this version posted November 7, 2024. The copyright holder for this preprint (which was not certified by peer review) is the author/funder, who has granted medRxiv a license to display the preprint in perpetuity.
It is made available under a CC-BY-NC 4.0 International license .

index measuring the strictness of containment policies in schools computed by OxCGRT [39]. It takes integer values from 0 (i.e., no containment measures are in place) to 3 (i.e, full school closure). Notably, contacts at home are not adjusted although we acknowledge they may increase due to the adoption of NPIs.

Modelling multiple viral strains

In order to capture the spread of a second variant in British Columbia, Lombardy, and São Paulo, we introduce new compartments L', I', R', D' and $D^{o'}$ for non-vaccinated individuals infected by a second strain. Similarly, we consider compartments $L^{V'}$, $I^{V'}$, $R^{V'}$, $D^{V'}$, $D^{oV'}$ for vaccinated individuals infected by a VOC. We model the introduction of a second variant as follows. We denote t_{var} as the time at which the second variant establishes its presence in each location. To this end, we use genomics data from Ref. [40] and calibrate t_{var} in a range between 0 and 42 days prior to the first date in which each variant is consistently featured in the genomics data (i.e., the share of the variant in the genomics data is different than zero from this first date onwards). We did not consider the first appearance in the dataset as a single sample might be linked to an isolated importation from a different location. Then, during simulations at t_{var}, we initialize the compartment I' by allocating there 1% of infected individuals (considering both I and I_V).

The four regions studied faced the Alpha, the Gamma, and the Delta VOC. In detail, in British Columbia and Lombardy, Alpha appeared as second strain replacing the wild type. In London, the Alpha variant was the dominant variant circulating throughout our time horizon. In São Paulo, the initial variant observed at the start of the simulation period was Gamma which was then replaced by Delta.

We model VOC by adjusting (or not) relevant parameters. According to literature, the latent period of Alpha and Gamma is similar to that of the wild type [47–50]. Hence, we keep $\epsilon' = 4^{-1} days^{-1}$ for these variants. In contrast, the latent period of Delta has been reported to be shorter [51]. Hence, we set $\epsilon' = 3^{-1} days^{-1}$ for this VOC. For all variants, including the wild type, we set the infectious period to $\mu = 2.5^{-1} days^{-1}$. Additionally, the second variant may exhibit higher transmissibility. Thus we adjust the transmissibility of variants by multiplying it by a parameter σ, which represents the relative increase in transmissibility. Following the literature we set $\sigma = 1.5$ for Alpha compared to the wild type [43]. For São Paulo, where Delta replaced Gamma, we calibrate σ in a range of $[1.6 - 2.5]$, as no specific indication was found in the literature. Moreover, the vaccine efficacy might also be lower against variants [43, 45, 46]. Following the literature, we set the vaccine efficacy as $VE = 90\%$ (VE_S=85%) against the wild type [45], $VE = 85\%$ ($VE_S = 75\%$) against Alpha [45], $VE = 80\%$ ($VE_S = 65\%$) against Gamma [46], and $VE = 90\%$ ($VE_S = 60\%$) against Delta [45].

medRxiv preprint doi: https://doi.org/10.1101/2024.11.07.24316893; this version posted November 7, 2024. The copyright holder for this preprint (which was not certified by peer review) is the author/funder, who has granted medRxiv a license to display the preprint in perpetuity.
It is made available under a CC-BY-NC 4.0 International license .

Behavioural models

Building on the baseline and the literature, we implemented four additional models that also include behavioural relaxation mechanisms [27, 28]. To this end, we introduce new compartments S_{NC} and S^V_{NC} to account for susceptible individuals (vaccinated or not) that relax adoption of NPIs becoming non-compliant (NC). In detail, individuals who relax their behaviour transit from S (S^V) to S_{NC} (S^V_{NC}). Conversely, non-compliant individuals who return to compliant behaviours transition from S_{NC} (S^V_{NC}) to S (S^V). We assume that individuals in the non-compliant compartments get infected at higher rates compared to those in compliant compartments [23, 24]. This is accounted for by multiplying their force of infection by a factor $r > 1$.

Following the literature, we study four different behavioural models that differ in the mechanisms used to describe how individuals enter and leave the non-compliant compartments. In model 1, susceptible individuals (vaccinated or not) can enter or leave the NC compartments at constant rates α and γ. In model 2, susceptible individuals enter or leave the NC compartment at varying rates. The transition rate from S (S^V) to S_{NC} (S^V_{NC}) is set as a function of the fraction of vaccinated individuals and a parameter α. The transition rate from S_{NC} (S^V_{NC}) to S (S^V) is set as a function of the number of reported daily deaths per $100,000$ and a parameter γ. Model 3 and model 4 are analogous to model 1 and 2. However, only vaccinated individuals can transition to the NC compartment. The structure of our models is illustrated in Fig. 5. More details are reported in the Supporting Information.

Models calibration

We apply an Approximate Bayesian Computation-Sequential Monte Carlo(ABC-SMC) method to calibrate our models [32] to reported data. The goal of ABC-SMC algorithm is to estimate the posterior distribution of free parameters $\boldsymbol{\theta}$ starting from an input prior distribution $P(\boldsymbol{\theta})$. It is an extension of the ABC rejection algorithm, where suitable parameters are found by iteratively sampling a prior distribution and computing for each sampled parameter $\boldsymbol{\theta}_i$ a distance function $d(\mathbf{y}_i, \mathbf{y}_{data})$, where $\mathbf{y}_i \sim f(\boldsymbol{\theta}_i)$ is the output of the model and $\mathbf{y}_{data}$ is the reported data (i.e., weekly deaths). Each $\boldsymbol{\theta}_i$ is accepted if $d(\mathbf{y}_i, \mathbf{y}_{data}) \leq \epsilon$, where ϵ is a predefined tolerance. The process is repeated until M parameters $\boldsymbol{\theta}_i$ are accepted. Their distribution approximates the true posterior distribution $\Pi(\boldsymbol{\theta}|\mathbf{y}_{data}, \epsilon)$. The ABC rejection algorithm is of straightforward implementation, however suffers from several limitations. First, the values of M and of the tolerance ϵ are free parameters that shape the interplay between convergence speed and accuracy [63]. Second, the prior distribution is never updated to account for information from previous iterations. The ABC-SMC framework has been developed to tackle these issues. It consists of T generations (i.e., iterations). The first one is based on a rejection algorithm step where ϵ is set to a high value. In the second generation, the tolerance is decreased parameters are sampled from those accepted in the previous step and perturbed via a kernel to avoid converging on local minima of the phase space.

medRxiv preprint doi: https://doi.org/10.1101/2024.11.07.24316893; this version posted November 7, 2024. The copyright holder for this preprint (which was not certified by peer review) is the author/funder, who has granted medRxiv a license to display the preprint in perpetuity.
It is made available under a CC-BY-NC 4.0 International license .

The process is repeated for T generations of M particles (i.e, samples) each. Then, the set of accepted parameters in the last generation is used as the empirical posterior distribution. We adopted a python implementation of ABC-SMC from the library pyabc [64].

The free parameters and the priors explored in our models are:

- Reproductive number R_0. We explore values in the interval $[1, 3]$.
- Delay in reporting deaths Δ. Consistent with observations, we explore the interval $[3, 64]$ [65].
- Initial fraction of infections of the total population i_{ini}. We estimating the ranges from the number of deaths and IFR across the four regions. We explore the interval $[0.0005, 0.02]$.
- Initial fraction of individuals with residual immunity from past waves r_{ini}. We explore the range of $[0.1, 0.4]$.
- Start date t_0 of the simulation of epidemic. We calibrate t_0 within a range of 8 weeks such that $t_0 = t^* - \Delta t$, where $\Delta t = [0, 1, \ldots, 7]$ week(s). The baseline dates t^* are set as 8 weeks before the peak of mortality in real data. Following this, t^* is set as 2020/10/12 for British Columbia, 2020/10/05 for Lombardy, 2020/11/16 for London, and 2021/01/18 for São Paulo.
- Introduction date of a VOC t_{var} (applied for all regions except London). we use genomics data from Ref. [40] and calibrate t_{var} in a range between 0 and 42 days prior to the first date t^*_{var} from which each variant is consistently featured in the genomics data. Thus, $t_{var} = t^*_{var} - \Delta t_{var}$, where $\Delta t_{var} = [0, 1, \ldots, 42]$ day(s). t^*_{var} is set as 2020/12/21 in British Columbia, 2020/9/28 in Lombardy, and 2021/3/29 in São Paulo.
- Relative transmissibility σ of Delta with respect to Gamma. In the case of São Paulo, Delta replaced Gamma. Literature shows that Delta is about 1.3 times more transmissible than Gamma [42]. We explore the interval $[1.0 - 2.5]$.
- Behavioural parameters α and γ. We explore the interval $[0.0001 - 10]$. For both and sample them on a logarithmic scale.
- Relative infection probability of non-compliant individuals r. Individuals who relax their behaviour are more likely infected. Therefore, we increase the infection probability of non-compliant individuals by multiplying it by a factor r. We explore the interval $[1.0, 1.5]$.

The initial prior distribution $P(\boldsymbol{\theta})$ is obtained sampling each interval uniformly.

medRxiv preprint doi: https://doi.org/10.1101/2024.11.07.24316893; this version posted November 7, 2024. The copyright holder for this preprint (which was not certified by peer review) is the author/funder, who has granted medRxiv a license to display the preprint in perpetuity.
It is made available under a CC-BY-NC 4.0 International license .

Model initialization

We initialize the number of individuals in each compartment as follows. We assume that, at the beginning, all individuals are in the compartments S or L or I or R. The initial individual numbers of infected (including both L and I compartments) and recovered (R) individuals are set as fractions of total population considering under-reporting and official data. The total number of infected individuals is then distributed to L and I compartments proportionally to the inverse of their respective transition rates. Besides, since our model is age-stratified, the initial numbers of individuals in compartments S (L or I or R) in each age group is set as $N_S \times N_k/N$ ($N_L \times N_k/N$ or $N_I \times N_k/N$ or $N_R \times N_k/N$), where N_k is the individual number in age-group k, N is the total individual number, N_S is the total number of individuals in compartment S. All parameters of our models are displayed in Table 4.

Table 4. Model parameters.

Parameter	**Symbol**	**Value**
Reproductive number	R_0	Calibrated within $[1, 3]$.
Latent period	ϵ	$3^{-1}days^{-1}$ for Delta [51], $4^{-1}days^{-1}$ for others[47–50]
Infectious period	μ	$2.5^{-1}days^{-1}$ [47, 66]
Transmission rate	β	Obtained from R_0
Infection fatality rate	IFR	Ref.[57]
Contact matrix	$\mathbf{C}$	Ref. [61]
Delayed days in reporting deaths	Δ	Calibrated within $[3, 64]$ [65]
Initial fraction of infections	i_{ini}	Calibrated within $[0.0005, 0.02]$
Initial fraction of recoveries	r_{ini}	Calibrated within $[0.1, 0.4]$
Adjustment of the start date of the simulation of epidemic with respect to the baseline date (t^*)	Δt	Calibrated within $[0, 7]$ weeks
Adjustment of the introduction date of a VOC with respect to the date (t^*_{var}) at which each variant is consistently featured in the genomics data	Δt_{var}	Calibrated within $[0, 42]$ days [67]
Relative transmissibility of a second variant	σ	1.5 for Alpha [43]; calibrated within $[1.0 - 2.5]$ for Delta with respect to Gamma [42]
Overall vaccine efficacy	VE	0.9 against wild type and Delta variant; 0.85 against Alpha variant; 0.8 against Gamma variant [45, 46]
Vaccine efficacy against infection	VE_S	0.85 against wild type; 0.6 against Delta variant; 0.75 against Alpha variant; 0.65 against Gamma variant[45, 46]
Transition rate towards non-compliance	α	Calibrated within $[0.0001 - 10]$
Transition rate towards compliance	γ	Calibrated within $[0.0001 - 10]$
Relative infection risk of non-compliant individuals	r	Calibrated within $[1.0 - 1.5]$

Models evaluation

We utilize weighted mean absolute percentage errors (wMAPEs) and Akaike Information Criteria (AIC) scores [56] for evaluating the five models. wMAPE measures the difference between the median outcomes

medRxiv preprint doi: https://doi.org/10.1101/2024.11.07.24316893; this version posted November 7, 2024. The copyright holder for this preprint (which was not certified by peer review) is the author/funder, who has granted medRxiv a license to display the preprint in perpetuity.
It is made available under a CC-BY-NC 4.0 International license .

of our models and reported data. It is defined as:

$$\text{wMAPE} = \frac{\sum_{t=1}^{t_f} |y_{data,t} - median(y_{i,t})|}{\sum_{i=t}^{t_f} y_{data,t}} \tag{3}$$

where $y_{data,t}$ is the reported data at time t, $median(y_{i,t})$ is median trajectory of model i at time t, and t_f is the total number of weeks.

AIC scores assess the performance by trading off the complexity and fitting of the models. The AIC score of model i is computed as:

$$AIC_i = t_f log\Phi^2 + 2K_i \tag{4}$$

where Φ^2 is the sum of the squares of residuals, t_f is the number of data points (i.e., weeks considered), and K_i is the number of free parameters of model i. To obtain a more intuitive metric, we calculate Akaike weights from the AIC scores. These can be interpreted as the relative likelihood of a given model [31]. The Akaike weight of model i, denoted by w_i, is computed as

$$w_i = \frac{e^{-\Delta AIC_i/2}}{\sum_{i=1}^{Q} e^{-\Delta AIC_i/2}} \tag{5}$$

where ΔAIC_i is the difference between the AIC score of model i and of the best model (i.e., the one with lowest AIC score), and Q is the number of models.

Relative deaths difference

To quantify the effect of vaccination, NPIs or behavioural relaxation on deaths, we compute the relative deaths difference (RDD) as the relative difference between the total number of deaths as simulated by the original model and in a counterfactual scenario where vaccinations, NPIs, or behavioural relaxation are removed. The relative deaths difference is calculated as:

$$RDD = \frac{D_{counterfactual} - D_{original}}{D_{counterfactual}} \times 100\% \tag{6}$$

where $D_{original}$ and $D_{counterfactual}$ are the total number of deaths simulated in the original model and in the counterfactual scenario, respectively. The same approach, applied to infections, is used to compute the relative different of infections (RDI).

Acknowledgments

Y.L. acknowledges support from the China Scholarship Council (CSC). N.G. acknowledges support from the Lagrange Project of the Institute for Scientific Interchange Foundation (ISI Foundation) funded by

medRxiv preprint doi: https://doi.org/10.1101/2024.11.07.24316893; this version posted November 7, 2024. The copyright holder for this preprint (which was not certified by peer review) is the author/funder, who has granted medRxiv a license to display the preprint in perpetuity.
It is made available under a CC-BY-NC 4.0 International license .

Fondazione Cassa di Risparmio di Torino (Fondazione CRT). All authors thank the High Performance Computing facilities at Queen Mary University of London.

Author Contributions

Y.L., N.G, and N.P. designed the research. Y.L. performed the simulations. Y.L., and N.P. wrote the first draft of the manuscript. All authors contributed interpreting the data, editing and approving the manuscript.

Data and code

The data and code to replicate the results can be found in `https://github.com/Jadecoool/Estimating-behavioural-relaxation-induced-by-COVID-19-vaccines-in-the-first-months-of-their-rollout/tree/main`

References

[1] Eleftheria Vasileiou, Colin R Simpson, Ting Shi, Steven Kerr, Utkarsh Agrawal, Ashley Akbari, Stuart Bedston, Jillian Beggs, Declan Bradley, Antony Chuter, et al. Interim findings from first-dose mass covid-19 vaccination roll-out and covid-19 hospital admissions in scotland: a national prospective cohort study. The Lancet, 397(10285):1646–1657, 2021.

[2] Noa Dagan, Noam Barda, Eldad Kepten, Oren Miron, Shay Perchik, Mark A Katz, Miguel A Hernán, Marc Lipsitch, Ben Reis, and Ran D Balicer. Bnt162b2 mrna covid-19 vaccine in a nationwide mass vaccination setting. New England Journal of Medicine, 384(15):1412–1423, 2021.

[3] Oliver J Watson, Gregory Barnsley, Jaspreet Toor, Alexandra B Hogan, Peter Winskill, and Azra C Ghani. Global impact of the first year of covid-19 vaccination: a mathematical modelling study. The Lancet infectious diseases, 22(9):1293–1302, 2022.

[4] David W Eyre, Donald Taylor, Mark Purver, David Chapman, Tom Fowler, Koen B Pouwels, A Sarah Walker, and Tim EA Peto. Effect of covid-19 vaccination on transmission of alpha and delta variants. New England Journal of Medicine, 386(8):744–756, 2022.

[5] Malik Sallam. Covid-19 vaccine hesitancy worldwide: a concise systematic review of vaccine acceptance rates. Vaccines, 9(2):160, 2021.

[6] Diego F Cuadros, Juan D Gutierrez, Claudia M Moreno, Santiago Escobar, F DeWolfe Miller, Godfrey Musuka, Ryosuke Omori, Phillip Coule, and Neil J MacKinnon. Impact of healthcare

medRxiv preprint doi: https://doi.org/10.1101/2024.11.07.24316893; this version posted November 7, 2024. The copyright holder for this preprint (which was not certified by peer review) is the author/funder, who has granted medRxiv a license to display the preprint in perpetuity.
It is made available under a CC-BY-NC 4.0 International license .

capacity disparities on the covid-19 vaccination coverage in the united states: a cross-sectional study. The Lancet Regional Health–Americas, 18, 2023.

[7] Ahmed Mushfiq Mobarak, Edward Miguel, Jason Abaluck, Amrita Ahuja, Marcella Alsan, Abhijit Banerjee, Emily Breza, Arun G Chandrasekhar, Esther Duflo, James Dzansi, et al. End covid-19 in low-and middle-income countries. Science, 375(6585):1105–1110, 2022.

[8] Yuqi Duan, Junyi Shi, Zongbin Wang, Shuduo Zhou, Yinzi Jin, and Zhi-Jie Zheng. Disparities in covid-19 vaccination among low-, middle-, and high-income countries: the mediating role of vaccination policy. Vaccines, 9(8):905, 2021.

[9] Sam Moore, Edward M Hill, Michael J Tildesley, Louise Dyson, and Matt J Keeling. Vaccination and non-pharmaceutical interventions for covid-19: a mathematical modelling study. The lancet infectious diseases, 21(6):793–802, 2021.

[10] Nicolò Gozzi, Matteo Chinazzi, Natalie E Dean, Ira M Longini Jr, M Elizabeth Halloran, Nicola Perra, and Alessandro Vespignani. Estimating the impact of covid-19 vaccine inequities: a modeling study. Nature Communications, 14(1):3272, 2023.

[11] Malik Sallam, Mariam Al-Sanafi, and Mohammed Sallam. A global map of covid-19 vaccine acceptance rates per country: an updated concise narrative review. Journal of multidisciplinary healthcare, pages 21–45, 2022.

[12] Sharifa Nasreen, Hannah Chung, Siyi He, Kevin A Brown, Jonathan B Gubbay, Sarah A Buchan, Deshayne B Fell, Peter C Austin, Kevin L Schwartz, Maria E Sundaram, et al. Effectiveness of covid-19 vaccines against symptomatic sars-cov-2 infection and severe outcomes with variants of concern in ontario. Nature microbiology, 7(3):379–385, 2022.

[13] John S Tregoning, Katie E Flight, Sophie L Higham, Ziyin Wang, and Benjamin F Pierce. Progress of the covid-19 vaccine effort: viruses, vaccines and variants versus efficacy, effectiveness and escape. Nature reviews immunology, 21(10):626–636, 2021.

[14] Nicolò Gozzi, Matteo Chinazzi, Jessica T Davis, Kunpeng Mu, Ana Pastore y Piontti, Marco Ajelli, Nicola Perra, and Alessandro Vespignani. Anatomy of the first six months of covid-19 vaccination campaign in italy. PLoS Computational Biology, 18(5):e1010146, 2022.

[15] Marta Galanti, Sen Pei, Teresa K Yamana, Frederick J Angulo, Apostolos Charos, David L Swerdlow, and Jeffrey Shaman. Social distancing remains key during vaccinations. Science, 371(6528):473–474, 2021.

[16] Nicola Perra. Non-pharmaceutical interventions during the covid-19 pandemic: A review. Physics Reports, 913:1–52, 2021.

medRxiv preprint doi: https://doi.org/10.1101/2024.11.07.24316893; this version posted November 7, 2024. The copyright holder for this preprint (which was not certified by peer review) is the author/funder, who has granted medRxiv a license to display the preprint in perpetuity.
It is made available under a CC-BY-NC 4.0 International license .

[17] Irwin M Rosenstock. The health belief model and preventive health behavior. Health education monographs, 2(4):354–386, 1974.

[18] Sylvie C Briand, Matteo Cinelli, Tim Nguyen, Rosamund Lewis, Dimitri Prybylski, Carlo M Valensise, Vittoria Colizza, Alberto Eugenio Tozzi, Nicola Perra, Andrea Baronchelli, et al. Infodemics: A new challenge for public health. Cell, 184(25):6010–6014, 2021.

[19] Janetta E Skarp, Laura E Downey, Julius WE Ohrnberger, Lucia Cilloni, Alexandra B Hogan, Abagael L Sykes, Susannah S Wang, Hiral Anil Shah, Mimi Xiao, and Katharina Hauck. A systematic review of the costs relating to non-pharmaceutical interventions against infectious disease outbreaks. Applied Health Economics and Health Policy, 19:673–697, 2021.

[20] Michele Tizzoni, Elaine O Nsoesie, Laetitia Gauvin, Márton Karsai, Nicola Perra, and Shweta Bansal. Addressing the socioeconomic divide in computational modeling for infectious diseases. Nature communications, 13(1):2897, 2022.

[21] Valeria d'Andrea, Riccardo Gallotti, Nicola Castaldo, and Manlio De Domenico. Individual risk perception and empirical social structures shape the dynamics of infectious disease outbreaks. PLOS Computational Biology, 18(2):e1009760, 2022.

[22] Zhiyuan Yu, David Gurarie, and Qimin Huang. Media-driven adaptive behavior in pandemic modeling and data analysis. medRxiv, pages 2024–04, 2024.

[23] Nicolò Gozzi, Paolo Bajardi, and Nicola Perra. The importance of non-pharmaceutical interventions during the covid-19 vaccine rollout. PLoS computational biology, 17(9):e1009346, 2021.

[24] Alexandra Teslya, Ganna Rozhnova, Thi Mui Pham, Daphne A van Wees, Hendrik Nunner, Noortje G Godijk, Martin Bootsma, and Mirjam E Kretzschmar. The importance of sustained compliance with physical distancing during covid-19 vaccination rollout. Communications medicine, 2(1):146, 2022.

[25] Diogo H Silva, Celia Anteneodo, and Silvio C Ferreira. Epidemic outbreaks with adaptive prevention on complex networks. Communications in Nonlinear Science and Numerical Simulation, 116:106877, 2023.

[26] Alessandro De Gaetano, Alain Barrat, and Daniela Paolotti. Modeling the interplay between disease spread, behaviors, and disease perception with a data-driven approach. medRxiv, pages 2024–04, 2024.

[27] James Wambua, Neilshan Loedy, Christopher I Jarvis, Kerry LM Wong, Christel Faes, Rok Grah, Bastian Prasse, Frank Sandmann, Rene Niehus, Helen Johnson, et al. The influence of covid-19 risk

medRxiv preprint doi: https://doi.org/10.1101/2024.11.07.24316893; this version posted November 7, 2024. The copyright holder for this preprint (which was not certified by peer review) is the author/funder, who has granted medRxiv a license to display the preprint in perpetuity.
It is made available under a CC-BY-NC 4.0 International license .

perception and vaccination status on the number of social contacts across europe: insights from the comix study. BMC Public Health, 23(1):1350, 2023.

[28] Honghan Bei, Peiyan Li, Zhi Cai, and Roberto Murcio. The impact of covid-19 vaccination on human mobility: The london case. Heliyon, 9(8), 2023.

[29] Alessandro De Gaetano, Paolo Bajardi, Nicolò Gozzi, Nicola Perra, Daniela Perrotta, and Daniela Paolotti. Behavioral changes associated with covid-19 vaccination: Cross-national online survey. Journal of Medical Internet Research, 25:e47563, 2023.

[30] Kathleen Mccoll, Dylan Martin-Lapoirie, Giuseppe A Veltri, Pierre Arwidson, and Jocelyn Raude. Does vaccination elicit risk compensation? insights from the covid-19 pandemic in france. Health Psychology and Behavioral Medicine, 12(1):2287663, 2024.

[31] Eric-Jan Wagenmakers and Simon Farrell. Aic model selection using akaike weights. Psychonomic bulletin & review, 11:192–196, 2004.

[32] Tina Toni, David Welch, Natalja Strelkowa, Andreas Ipsen, and Michael PH Stumpf. Approximate bayesian computation scheme for parameter inference and model selection in dynamical systems. Journal of the Royal Society Interface, 6(31):187–202, 2009.

[33] Government of canada. covid-19 vaccination: Vaccination coverage. DOI:https://health-infobase.canada.ca/covid-19/vaccination-coverage/.

[34] Covid-19 opendata vaccines. DOI:https://github.com/italia/covid19-opendata-vaccini/.

[35] Greater london authority. coronavirus (covid-19) weekly update. DOI:https://data.london.gov.uk/dataset/coronavirus--covid-19--cases.

[36] opendatasus, ministry of health. data & resources. DOI:https://opendatasus.saude.gov.br/dataset/covid-19-vacinacao.

[37] Leonardo Souto Ferreira, Flavia Maria Darcie Marquitti, Rafael Lopes Paixão da Silva, Marcelo Eduardo Borges, Marcelo Ferreira da Costa Gomes, Oswaldo Gonçalves Cruz, Roberto André Kraenkel, Renato Mendes Coutinho, Paulo Inácio Prado, and Leonardo Soares Bastos. Estimating the impact of implementation and timing of the covid-19 vaccination programme in brazil: a counterfactual analysis. The Lancet Regional Health–Americas, 17, 2023.

[38] Google llc "google covid-19 community mobility reports". DOI:https://www.google.com/covid19/mobility/.

[39] Oxford covid-19 government response tracker. DOI:https://www.bsg.ox.ac.uk/research/research-projects/coronavirus-government-response-tracker#data.

medRxiv preprint doi: https://doi.org/10.1101/2024.11.07.24316893; this version posted November 7, 2024. The copyright holder for this preprint (which was not certified by peer review) is the author/funder, who has granted medRxiv a license to display the preprint in perpetuity.
It is made available under a CC-BY-NC 4.0 International license .

[40] Emma B. Hodcroft. Covariants: Sars-cov-2 mutations and variants of interest. DOI:https://covariants.org/.

[41] Jun Yong Choi and Davey M Smith. Sars-cov-2 variants of concern. Yonsei medical journal, 62(11):961, 2021.

[42] Marta Giovanetti, Vagner Fonseca, Eduan Wilkinson, Houriiyah Tegally, Emmanuel James San, Christian L Althaus, Joilson Xavier, Svetoslav Nanev Slavov, Vincent Louis Viala, Alex Ranieri Jerônimo Lima, et al. Replacement of the gamma by the delta variant in brazil: Impact of lineage displacement on the ongoing pandemic. Virus evolution, 8(1):veac024, 2022.

[43] Diana Duong. Alpha, beta, delta, gamma: What's important to know about sars-cov-2 variants of concern?, 2021.

[44] Chun Huai Luo, C Paul Morris, Jaiprasath Sachithanandham, Adannaya Amadi, David Gaston, Maggie Li, Nicholas J Swanson, Matthew Schwartz, Eili Y Klein, Andrew Pekosz, et al. Infection with the sars-cov-2 delta variant is associated with higher infectious virus loads compared to the alpha variant in both unvaccinated and vaccinated individuals. MedRxiv, 2021.

[45] Julia Shapiro, Natalie E Dean, Zachary J Madewell, Yang Yang, M Elizabeth Halloran, and Ira Longini. Efficacy estimates for various covid-19 vaccines: what we know from the literature and reports. MedRxiv, pages 2021–05, 2021.

[46] Leonardo Souto Ferreira, Gabriel Berg de Almeida, Marcelo Eduardo Borges, Lorena Mendes Simon, Silas Poloni, Ângela Maria Bagattini, Michelle Quarti Machado da Rosa, José Alexandre Felizola Diniz Filho, Ricardo de Souza Kuchenbecker, Suzi Alves Camey, et al. Modelling optimal vaccination strategies against covid-19 in a context of gamma variant predominance in brazil. Vaccine, 40(46):6616–6624, 2022.

[47] Stephen M Kissler, Christine Tedijanto, Edward Goldstein, Yonatan H Grad, and Marc Lipsitch. Projecting the transmission dynamics of sars-cov-2 through the postpandemic period. Science, 368(6493):860–868, 2020.

[48] Hualei Xin, Yu Li, Peng Wu, Zhili Li, Eric HY Lau, Ying Qin, Liping Wang, Benjamin J Cowling, Tim K Tsang, and Zhongjie Li. Estimating the latent period of coronavirus disease 2019 (covid-19). Clinical Infectious Diseases, 74(9):1678–1681, 2022.

[49] Shi Zhao, Biao Tang, Salihu S Musa, Shujuan Ma, Jiayue Zhang, Minyan Zeng, Qingping Yun, Wei Guo, Yixiang Zheng, Zuyao Yang, et al. Estimating the generation interval and inferring the latent period of covid-19 from the contact tracing data. Epidemics, 36:100482, 2021.

medRxiv preprint doi: https://doi.org/10.1101/2024.11.07.24316893; this version posted November 7, 2024. The copyright holder for this preprint (which was not certified by peer review) is the author/funder, who has granted medRxiv a license to display the preprint in perpetuity.
It is made available under a CC-BY-NC 4.0 International license .

[50] Shujuan Ma, Jiayue Zhang, Minyan Zeng, Qingping Yun, Wei Guo, Yixiang Zheng, Shi Zhao, Maggie H Wang, and Zuyao Yang. Epidemiological parameters of coronavirus disease 2019: a pooled analysis of publicly reported individual data of 1155 cases from seven countries. Medrxiv, pages 2020–03, 2020.

[51] Baisheng Li, Aiping Deng, Kuibiao Li, Yao Hu, Zhencui Li, Yaling Shi, Qianling Xiong, Zhe Liu, Qianfang Guo, Lirong Zou, et al. Viral infection and transmission in a large, well-traced outbreak caused by the sars-cov-2 delta variant. Nature communications, 13(1):460, 2022.

[52] PHE. Investigation of novel SARS-CoV-2 variant. Variant of Concern 202012/01. Technical briefing 3. https://assets.publishing.service.gov.uk/government/uploads/system/uploads/attachment_data/file/950823/Variant_of_Concern_VOC_202012_01_Technical_Briefing_3_-_England.pdf, 2021. [Online; accessed 13-January-2021].

[53] Allan S Detsky and Isaac I Bogoch. Covid-19 in canada: experience and response to waves 2 and 3. Jama, 326(12):1145–1146, 2021.

[54] Cecília Artico Banho, Lívia Sacchetto, Guilherme Rodrigues Fernandes Campos, Cíntia Bittar, Fábio Sossai Possebon, Leila Sabrina Ullmann, Beatriz de Carvalho Marques, Gislaine Ceslestino Dutra da Silva, Marília Mazzi Moraes, Maisa Carla Pereira Parra, et al. Impact of sars-cov-2 gamma lineage introduction and covid-19 vaccination on the epidemiological landscape of a brazilian city. Communications medicine, 2(1):41, 2022.

[55] Nuno R Faria, Thomas A Mellan, Charles Whittaker, Ingra M Claro, Darlan da S Candido, Swapnil Mishra, Myuki AE Crispim, Flavia CS Sales, Iwona Hawryluk, John T McCrone, et al. Genomics and epidemiology of the p. 1 sars-cov-2 lineage in manaus, brazil. Science, 372(6544):815–821, 2021.

[56] Hirotugu Akaike. A new look at the statistical model identification. IEEE transactions on automatic control, 19(6):716–723, 1974.

[57] Robert Verity, Lucy C Okell, Ilaria Dorigatti, Peter Winskill, Charles Whittaker, Natsuko Imai, Gina Cuomo-Dannenburg, Hayley Thompson, Patrick GT Walker, Han Fu, et al. Estimates of the severity of coronavirus disease 2019: a model-based analysis. The Lancet infectious diseases, 20(6):669–677, 2020.

[58] Hien Lau, Tanja Khosrawipour, Piotr Kocbach, Hirohito Ichii, Jacek Bania, and Veria Khosrawipour. Evaluating the massive underreporting and undertesting of covid-19 cases in multiple global epicenters. Pulmonology, 27(2):110–115, 2021.

medRxiv preprint doi: https://doi.org/10.1101/2024.11.07.24316893; this version posted November 7, 2024. The copyright holder for this preprint (which was not certified by peer review) is the author/funder, who has granted medRxiv a license to display the preprint in perpetuity.
It is made available under a CC-BY-NC 4.0 International license .

[59] Adriana Manna, Lorenzo Dall'Amico, Michele Tizzoni, Márton Karsai, and Nicola Perra. Generalized contact matrices allow integrating socioeconomic variables into epidemic models. Science Advances, 10(41):eadk4606, 2024.

[60] Sudam Surasinghe, Swathi Nachiar Manivannan, Samuel V Scarpino, Lorin Crawford, and C Brandon Ogbunugafor. Structural causal influence (sci) captures the forces of social inequality in models of disease dynamics. arXiv preprint arXiv:2409.09096, 2024.

[61] Kiesha Prem, Alex R Cook, and Mark Jit. Projecting social contact matrices in 152 countries using contact surveys and demographic data. PLoS computational biology, 13(9):e1005697, 2017.

[62] Dina Mistry, Maria Litvinova, Ana Pastore y Piontti, Matteo Chinazzi, Laura Fumanelli, Marcelo FC Gomes, Syed A Haque, Quan-Hui Liu, Kunpeng Mu, Xinyue Xiong, et al. Inferring high-resolution human mixing patterns for disease modeling. Nature communications, 12(1):323, 2021.

[63] Amanda Minter and Renata Retkute. Approximate Bayesian Computation for infectious disease modelling. Epidemics, 29:100368, 2019.

[64] Yannik Schälte, Emmanuel Klinger, Emad Alamoudi, and Jan Hasenauer. pyabc: Efficient and robust easy-to-use approximate bayesian computation. Journal of Open Source Software, 7(74):4304, 2022.

[65] Covid-19 pandemic planning scenarios, cdc. DOI:https://www.cdc.gov/coronavirus/2019-ncov/hcp/planning-scenarios.html#table-1.

[66] Jantien A Backer, Don Klinkenberg, and Jacco Wallinga. Incubation period of 2019 novel coronavirus (2019-ncov) infections among travellers from wuhan, china, 20–28 january 2020. Eurosurveillance, 25(5):2000062, 2020.

[67] Shagun Sharma, Surabhi Shrivastava, Shankar B Kausley, Beena Rai, and Aniruddha B Pandit. Coronavirus: a comparative analysis of detection technologies in the wake of emerging variants. Infection, 51(1):1–19, 2023.

[68] Pauline Van den Driessche. Reproduction numbers of infectious disease models. Infectious disease modelling, 2(3):288–303, 2017.

[69] Statistics canada. table 17-10-0005-01 population estimates on july 1, by age and gender. DOI: https://doi.org/10.25318/1710000501-eng.

[70] Italian national institute of statistics. resident population on 1st january: By age. DOI:http://dati.istat.it/Index.aspx?QueryId=42869&lang=en#.

medRxiv preprint doi: https://doi.org/10.1101/2024.11.07.24316893; this version posted November 7, 2024. The copyright holder for this preprint (which was not certified by peer review) is the author/funder, who has granted medRxiv a license to display the preprint in perpetuity.
It is made available under a CC-BY-NC 4.0 International license .

[71] Nomis, office for national statistics (ons). population estimates - local authority based by five year age band. DOI:https://www.nomisweb.co.uk/datasets/pestnew.

[72] Brazilian institute of geography and statistics. tables - 2018 population projections for brazil and federation units by sex and age: 2010-2060. DOI:https://www.ibge.gov.br/en/statistics/social/population/18176-population-projection.html?lang=en-GB.

Supporting information

Epidemic models

All the epidemic models studied here are based and built on a baseline which is a stochastic age-stratified epidemic compartmental model that integrates vaccination, NPIs, and the emergence/spread of a second variant. We consider a Susceptible-Latent-Infected-Recovered (SLIR) compartmentalization with the addition of deaths. Individuals are grouped into 16 age brackets with a five-year interval (except for the last 75+ group). We use age-stratified Infection Fatality rates (IFR) from Ref. [57] and age-stratified contact matrices from Ref. [61]. The natural history of the disease is modelled as follow. Susceptible individuals (S) transition to the latent stage (L compartment) where they are infected but not yet infectious. We assume a force of infection (i.e., the rate at which S get infected) function of age, transmissibility of each strain, contact matrices, and NPIs (see below for details). Individuals stay in L for an average of ϵ^{-1} $days^{-1}$. After, they become infectious thus transitioning to the I compartment. After the infectious period μ^{-1}, individuals either recover with the probability $(1 - IFR_k)$ (transitioning to R) or die from the disease with probability IFR_k (transitioning to D), where k denotes the age-group. We also consider a delay of Δ days in reporting deaths. Therefore, individuals are moved to compartment D^o from D after Δ days, capturing the delay in deaths reporting.

We simulate the disease progression by using stochastic chain binomial processes in all models. For

medRxiv preprint doi: https://doi.org/10.1101/2024.11.07.24316893; this version posted November 7, 2024. The copyright holder for this preprint (which was not certified by peer review) is the author/funder, who has granted medRxiv a license to display the preprint in perpetuity.
It is made available under a CC-BY-NC 4.0 International license .

age group k the baseline model is defined by the following set of stochastic equations:

$$S_k(t+\delta t) = S_k(t) - Mult_1(S_k(t), \lambda_k, \lambda'_k) - Mult_2(S_k(t), \lambda_k, \lambda'_k) \tag{7}$$

$$L_k(t+\delta t) = Mult_1(S_k(t), \lambda_k, \lambda'_k) - Bin(L_k, \epsilon) \tag{8}$$

$$I_k(t+\delta t) = Bin(L_k, \epsilon) - Bin(I_k, \mu) \tag{9}$$

$$R_k(t+\delta t) = Bin(I_k, \mu)(1 - IFR_k) \tag{10}$$

$$D_k(t+\delta t) = Bin(I_k, \mu) IFR_k \tag{11}$$

$$D^o_k(t+\delta t) = D_k(t+\delta t - \Delta) \tag{12}$$

$$L'_k(t+\delta t) = Mult_2(S_k(t), \lambda_k, \lambda'_k) - Bin(L'_k, \epsilon) \tag{13}$$

$$I'_k(t+\delta t) = Bin(L'_k, \epsilon) - Bin(I'_k, \mu) \tag{14}$$

$$R'_k(t+\delta t) = Bin(I'_k, \mu)(1 - IFR_k) \tag{15}$$

$$D'_k(t+\delta t) = Bin(I'_k, \mu) IFR_k \tag{16}$$

$$D^{o\prime}_k(t+\delta t) = D'_k(t+\delta t - \Delta) \tag{17}$$

$$\begin{aligned} S^V_k(t+\delta t) = {} & S^V_k(t) - Mult_1(S^V_k(t), (1-VE_S)\lambda_k, (1-VE'_S)\lambda'_k) \\ & - Mult_2(S^V_k(t), (1-VE_S)\lambda_k, (1-VE'_S)\lambda'_k) \end{aligned} \tag{18}$$

$$L^V_k(t+\delta t) = Mult_1(S^V_k(t), (1-VE_S)\lambda_k, (1-VE'_S)\lambda'_k) - Bin(L^V_k, \epsilon) \tag{19}$$

$$I^V_k(t+\delta t) = Bin(L^V_k, \epsilon) - Bin(I^V_k, \mu) \tag{20}$$

$$R^V_k(t+\delta t) = Bin(I^V_k, \mu)(1 - (1-VE_M) IFR_k) \tag{21}$$

$$D^V_k(t+\delta t) = Bin(I^V_k, \mu)(1-VE_M) IFR_k \tag{22}$$

$$D^{oV}_k(t+\delta t) = D^V_k(t+\delta t - \Delta) \tag{23}$$

$$L^{V\prime}_k(t+\delta t) = Mult_2(S^V_k(t), (1-VE_S)\lambda_k, (1-VE'_S)\lambda'_k) - Bin(L^{V\prime}_k, \epsilon) \tag{24}$$

$$I^{V\prime}_k(t+\delta t) = Bin(L^{V\prime}_k, \epsilon) - Bin(I^{V\prime}_k, \mu) \tag{25}$$

$$R^{V\prime}_k(t+\delta t) = Bin(I^{V\prime}_k, \mu)(1 - (1-VE'_M) IFR_k) \tag{26}$$

$$D^{V\prime}_k(t+\delta t) = Bin(I^{V\prime}_k, \mu)(1-VE'_M) IFR_k \tag{27}$$

$$D^{oV\prime}_k(t+\delta t) = D^{V\prime}_k(t+\delta t - \Delta) \tag{28}$$

where the force of infection of the original strain is

$$\lambda_k = \beta \sum_{j=1}^{N_k} \frac{\mathbf{C'}_{kj}(I_j + I^V_j)}{N_j} \tag{29}$$

medRxiv preprint doi: https://doi.org/10.1101/2024.11.07.24316893; this version posted November 7, 2024. The copyright holder for this preprint (which was not certified by peer review) is the author/funder, who has granted medRxiv a license to display the preprint in perpetuity.
It is made available under a CC-BY-NC 4.0 International license .

while is the force of infection of the second strain (if any) is

$$\lambda_k^{'} = \sigma\beta \sum_{j=1}^{N_k} \frac{\mathbf{C'}_{kj}(I_j^{'} + I_j^{V'})}{N_j} \tag{30}$$

β is the transmission rate of the first strain, σ indicates the relative transmissibility of the second strain compared to the previously circulating one. $\mathbf{C'}$ is the contact matrix adjusted for NPIs. To avoid issues with transition probabilities large than one, we transform the rates λ_k and $\lambda_k^{'}$ with the function $f(\lambda) = 1 - e^{-\lambda}$. Furthermore, $Mult_1(X, p_1, p_2)$ and $Mult_2(X, p_1, p_2)$ describe, respectively, a draw from the random variable 1 occurring with probability p_1 and the random variable 2 occurring with probability p_2, given X trials.

In the behavioural models we add non-compliant compartments. In models 1 and 2 non vaccinated and vaccinated susceptible can both become non-compliant (transitioning to, respectively, S_{NC} and S_{NC}^V). In models 3 and 4 the behavioural relaxation is linked only to vaccinated susceptible individuals.

medRxiv preprint doi: https://doi.org/10.1101/2024.11.07.24316893; this version posted November 7, 2024. The copyright holder for this preprint (which was not certified by peer review) is the author/funder, who has granted medRxiv a license to display the preprint in perpetuity.
It is made available under a CC-BY-NC 4.0 International license .

The transitions among compartments in models 1 and 2 are as following:

$$\begin{aligned}
S_k(t+\delta t) &= S_k(t) - Mult_1(S_k(t), \lambda_k, \lambda'_k, h(\alpha)) - Mult_2(S_k(t), \lambda_k, \lambda'_k, h(\alpha)) \\
&\quad - Mult_3(S_k(t), \lambda_k, \lambda'_k, h(\alpha)) + Mult_3({S^{NC}}_k(t), r\lambda_k, r\lambda'_k, h(\gamma)) \qquad (31)\\
{S^{NC}}_k(t+\delta t) &= {S^{NC}}_k(t) - Mult_1({S^{NC}}_k(t), r\lambda_k, r\lambda'_k, h(\gamma)) - Mult_2({S^{NC}}_k(t), r\lambda_k, r\lambda'_k, h(\gamma)) \\
&\quad - Mult_3({S^{NC}}_k(t), r\lambda_k, r\lambda'_k, h(\gamma)) + Mult_3(S_k(t), \lambda_k, \lambda'_k, h(\alpha)) \qquad (32)\\
L_k(t+\delta t) &= Mult_1(S_k(t), \lambda_k, \lambda'_k) + Mult_1(S_{NCk}(t), r\lambda_k, r\lambda'_k, h(\gamma)) - Bin(L_k, \epsilon) \qquad (33)\\
L'_k(t+\delta t) &= Mult_2(S'_k(t), \lambda_k, \lambda'_k) + Mult_2(S_{NCk}(t), r\lambda_k, r\lambda'_k, h(\gamma)) - Bin(L'_k, \epsilon) \qquad (34)\\
S^V_k(t+\delta t) &= S^V_k(t) - Mult_1(S^V_k(t), (1-VE_S)\lambda_k, (1-VE'_S)\lambda'_k, h(\alpha)) \\
&\quad - Mult_2(S^V_k(t), (1-VE_S)\lambda_k, (1-VE'_S)\lambda'_k, h(\alpha)) \\
&\quad - Mult_3(S^V_k(t), (1-VE_S)\lambda_k, (1-VE'_S)\lambda'_k, h(\alpha)) \\
&\quad + Mult_3(S^V_{NCk}(t), r(1-VE_S)\lambda_k, r(1-VE'_S)\lambda'_k, h(\gamma)) \qquad (35)\\
S^V_{NCk}(t+\delta t) &= S^V_{NCk}(t) - Mult_1(S^V_{NCk}(t), r(1-VE_S)\lambda_k, r(1-VE'_S)\lambda'_k, h(\gamma)) \\
&\quad - Mult_2(S^V_{NCk}(t), r(1-VE_S)\lambda_k, r(1-VE'_S)\lambda'_k, h(\gamma)) \\
&\quad - Mult_3(S^V_{NCk}(t), r(1-VE_S)\lambda_k, r(1-VE'_S)\lambda'_k, h(\gamma)) \\
&\quad + Mult_3(S^V_k(t), (1-VE_S)\lambda_k, (1-VE'_S)\lambda'_k, h(\alpha)) \qquad (36)\\
L^V_k(t+\delta t) &= Mult_1(S^V_k(t), (1-VE_S)\lambda_k, (1-VE'_S)\lambda'_k, h(\alpha)) \\
&\quad + Mult_1(S^V_{NCk}(t), r(1-VE_S)\lambda_k, r(1-VE'_S)\lambda'_k, h(\gamma)) - Bin(L^V_k, \epsilon) \qquad (37)\\
{L^V_k}'(t+\delta t) &= Mult_2(S^V_k(t), (1-VE_S)\lambda_k, (1-VE'_S)\lambda'_k, h(\alpha)) \\
&\quad + Mult_2(S^V_{NCk}(t), r(1-VE_S)\lambda_k, r(1-VE'_S)\lambda'_k, h(\gamma)) - Bin({L^V_k}', \epsilon) \qquad (38)
\end{aligned}$$

The transitions of the rest compartments are the same as those in the baseline model, described by Eqs 9-28.

Models 3 and 4 can be described by Eqs. 35-38, 7-17, 20-23, and 25-28.

R_0 calculation

We calculate the basic reproductive number R_0 of proposed model using the next generation matrix approach [68]. By definition, R_0 is the reproductive number at the beginning of the epidemics. Although our models include the emergence of a second variant, vaccines, and relaxation of individual behaviours, all of these become relevant only after the start of the epidemic. As such they have no influence on R_0. Thus, we can disregard the compartments related to the second variant, vaccination, and behavioural relaxation when we calculate R_0. We consider only the infected individuals in the compartments L_k and

medRxiv preprint doi: https://doi.org/10.1101/2024.11.07.24316893; this version posted November 7, 2024. The copyright holder for this preprint (which was not certified by peer review) is the author/funder, who has granted medRxiv a license to display the preprint in perpetuity.
It is made available under a CC-BY-NC 4.0 International license .

I_k. The deterministic equations regulating the dynamics of these two compartments are:

$$\frac{dL_k}{dt} = \lambda_k S_k - \epsilon L_k \tag{39}$$

$$\frac{dI_k}{dt} = \epsilon_k L_k - \mu I_k \tag{40}$$

We have $K = 16$ age groups, thus both Eqs. 39 and 40 contains K equations for different age groups. We describe these $2K$ equations in matrix form:

$$\begin{bmatrix} \frac{dL_1}{dt} \\ \vdots \\ \frac{dL_k}{dt} \\ \frac{dI_1}{dt} \\ \vdots \\ \frac{dI_k}{dt} \end{bmatrix} = \begin{bmatrix} \lambda_1 S_1 \\ \vdots \\ \lambda_k S_k \\ 0 \\ \vdots \\ 0 \end{bmatrix} - \begin{bmatrix} \epsilon L_1 \\ \vdots \\ \epsilon L_k \\ -\epsilon L_1 + \mu I_1 \\ \vdots \\ -\epsilon L_k + \mu I_k \end{bmatrix} \tag{41}$$

where $\lambda_k = \beta \sum_{j=1}^{N_k} \mathbf{C'}_{kj} I_j / N_j$ is the force of infection of the original strain, and the contact matrix $\mathbf{C'}$ accounts for the change in contacts induced by NPIs. We further denote Eq. 41 as

$$\begin{bmatrix} \frac{d\theta_1}{dt} \\ \vdots \\ \frac{d\theta_k}{dt} \\ \frac{d\theta_{k+1}}{dt} \\ \vdots \\ \frac{d\theta_{2k}}{dt} \end{bmatrix} = \begin{bmatrix} F_1 \\ \vdots \\ F_k \\ 0 \\ \vdots \\ 0 \end{bmatrix} - \begin{bmatrix} V_1 \\ \vdots \\ V_k \\ V_{k+1} \\ \vdots \\ V_{2k} \end{bmatrix} \tag{42}$$

For age group k, we consider the disease free equilibrium (DFE), defined as (S_k, L_k, I_k, R_k)=(N_k, 0, 0, 0). Next, we define two matrices: $\mathbf{F}_{ij}|_{DFE} = \frac{dF_i}{d\theta_j}$, $\mathbf{V}_{ij}|_{DFE} = \frac{dV_i}{d\theta_j}$. Considering the DFE, we write down $\mathbf{F}$ and $\mathbf{V}$ as follows.

$$F = \begin{bmatrix} 0 & \cdots & 0 & \frac{\beta N_1 C'_{1K} \chi}{N_K} & \cdots & \frac{\beta N_1 C'_{1K} \chi}{N_K} \\ \vdots & \ddots & \vdots & \vdots & \ddots & \vdots \\ 0 & \cdots & 0 & \frac{\beta N_K C'_{K1} \chi}{N_K} & \cdots & \frac{\beta N_K C'_{K1} \chi}{N_1} \\ 0 & \cdots & 0 & 0 & \cdots & 0 \\ \vdots & \ddots & \vdots & \vdots & \ddots & \vdots \\ 0 & \cdots & 0 & 0 & \cdots & 0 \end{bmatrix} \tag{43}$$

medRxiv preprint doi: https://doi.org/10.1101/2024.11.07.24316893; this version posted November 7, 2024. The copyright holder for this preprint (which was not certified by peer review) is the author/funder, who has granted medRxiv a license to display the preprint in perpetuity.
It is made available under a CC-BY-NC 4.0 International license .

$$V = \begin{bmatrix} \epsilon & \cdots & 0 & 0 & \cdots & 0 \\ \vdots & \ddots & \vdots & \vdots & \ddots & \vdots \\ 0 & \cdots & \epsilon & 0 & \cdots & 0 \\ -\epsilon & \cdots & 0 & \mu & \cdots & 0 \\ \vdots & \ddots & \vdots & \vdots & \ddots & \vdots \\ 0 & \cdots & -\epsilon & 0 & \cdots & \mu \end{bmatrix} \tag{44}$$

The reproductive number R_0 is defined as $\rho(\mathbf{FV^{-1}})$, where $\rho(\cdot)$ represents the spectral radius. Then, we write $\mathbf{F}$ and $\mathbf{V}^{-1}$ in blocks and we compute $\mathbf{V^{-1}}$ as follows:

$$\mathbf{F} = \begin{bmatrix} 0 & \beta\tilde{\mathbf{C}}' \\ 0 & 0 \end{bmatrix} \tag{45}$$

where $\tilde{\mathbf{C}}'$ indicates the adjusted contact matrix ($\tilde{\mathbf{C}}'_{ij} = \mathbf{C}'_{ij}\frac{N_i}{N_j}$) with a size of $K \times K$, and 0 indicates a $K \times K$ matrix with all zero elements.

$$\mathbf{V} = \begin{bmatrix} \epsilon\mathbb{1} & 0 \\ -\epsilon\mathbb{1} & \mu\mathbb{1} \end{bmatrix} \tag{46}$$

where $\mathbb{1}$ indicates a $K \times K$ identity matrix. Then we compute $\mathbf{V^{-1}}$

$$\mathbf{V^{-1}} = \begin{bmatrix} \frac{1}{\epsilon}\mathbb{1} & 0 \\ \frac{1}{\mu}\mathbb{1} & \frac{1}{\mu}\mathbb{1} \end{bmatrix} \tag{47}$$

Then, we obtain $\mathbf{FV^{-1}}$

$$\mathbf{FV^{-1}} = \begin{bmatrix} 0 & \beta\tilde{\mathbf{C}}' \\ 0 & 0 \end{bmatrix} \begin{bmatrix} \frac{1}{\epsilon}\mathbb{1} & 0 \\ \frac{1}{\mu}\mathbb{1} & \frac{1}{\mu}\mathbb{1} \end{bmatrix} = \begin{bmatrix} \frac{\beta\tilde{C}'}{\mu} & \frac{\beta\tilde{C}'}{\mu} \\ 0 & 0 \end{bmatrix} \tag{48}$$

Finally, we are left with finding the spectral radius of $\mathbf{FV^{-1}}$ (i.e., finding its largest eigenvalue). The eigenvalue problem can be written as $det(\mathbf{FV^{-1}} - \lambda\mathbb{1}) = 0$. Given the structure of $\mathbf{FV^{-1}}$, and since we are interested in non-trivial solutions (λ not equal to 0), the problem reduces to:

$$det(\frac{\beta\tilde{\mathbf{C}}'}{\mu} - \lambda\mathbb{1}) = 0 \tag{49}$$

Therefore, we obtain $R_0 = \rho(\mathbf{FV^{-1}}) = \frac{\beta}{\mu}\rho(\tilde{\mathbf{C}}')$.

Demographics of regions considered

Here, we provide more information about the demographic profiles of the four regions under study.

medRxiv preprint doi: https://doi.org/10.1101/2024.11.07.24316893; this version posted November 7, 2024. The copyright holder for this preprint (which was not certified by peer review) is the author/funder, who has granted medRxiv a license to display the preprint in perpetuity.
It is made available under a CC-BY-NC 4.0 International license .

Contact matrices

We first present the contact patterns among different age groups. In Fig. 6, we show the pre-Pandemic contact matrices of each region in four settings (i.e., home, school, work places, and other places) sourced from Ref. [61]. Across settings and regions we use the same colour scale for comparison. The plot shows that, across the board, the four regions exhibit similar contact patterns. In detail, the contacts at home show a higher intensity along the diagonal. Contacts at school are the most intense compared to the other three settings, where interactions are mainly among children and adolescents (i.e., age brackets $0-4$, $5-94$, $10-14$, $15-19$). This is followed by contacts at other places among the young population (i.e., $10-14$, $15-19$, $20-24$, $25-29$). Contacts at workplaces are less intense than in schools and other places, and are reported mainly among the middle-aged population. By considering contacts across all four settings, we obtain the aggregated contact matrices shown in the last column. The darker colour of the diagonal suggests that within-group interactions (i.e., among people in the same age group) are significantly more frequent than interactions across different age groups. Additionally, teenagers and young adults tend to have more contacts than the elderly population. To compare the contact matrices of the four regions, we compute the spectral radius of the aggregated contact matrix. We find that the spectral radius is 15.2 in British Columbia, 17.0 in Lombardy, 11.7 in London, and 19.5 in São Paulo. As discussed in the previous section, this indicates that, in the context of epidemic spreading, for a given disease London would feature the lowest R_0 while São Paulo the largest.

Contact intensity and population distribution

In Fig. 7 we show the pre-Pandemic contact intensity (panel A) and age distribution (panel B) for each age group in the four regions. Contact intensity is computed by summing each column of the overall contact matrix.

Younger age groups, particularly children and adolescents, exhibit the highest contact intensity across all regions, while the elderly population (i.e., 65+) the lowest. In detail, contact intensity peaks in the $15-19$ age group, followed by a general decline with age with small fluctuations including a slight increase in the $35-39$ age group (except in São Paulo, where the decline is consistent). A downward trend in contact intensity is observed from the $40-44$ age group onwards in all regions.

Fig. 7-B shows the population distributions of the four regions in 2021 [69–72]. In British Columbia, the population is relatively evenly distributed across most age groups, with small double peeks in the $30-34$ to $55-59$ age groups. Lombardy shows a gradual increase in population from the $30-34$ age group to the $50-54$ age group. The population distribution in London peaks in the $30-34$ age group, suggesting a substantial proportion of young adults. São Paulo shows a peak in the $35-39$ age group. Comparing the population distributions of the four regions, British Columbia and Lombardy display signs of ageing and also display smaller populations in younger age categories (i.e., $0-4$, $5-9$ age

medRxiv preprint doi: https://doi.org/10.1101/2024.11.07.24316893; this version posted November 7, 2024. The copyright holder for this preprint (which was not certified by peer review) is the author/funder, who has granted medRxiv a license to display the preprint in perpetuity.
It is made available under a CC-BY-NC 4.0 International license .

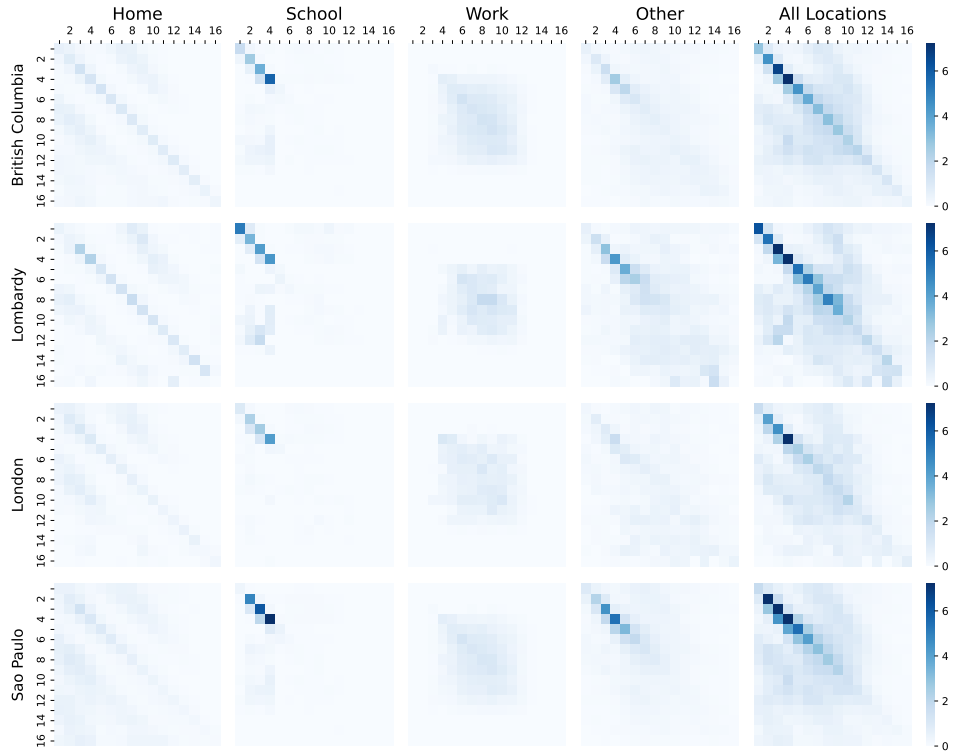

Fig 6. Contact matrices of the four regions. We show the four layers (i.e., home, school, workplace, and other places) of contact matrices between 16 age groups in each region (British Columbia, Lombardy, London, São Paulo). The numbers shown on the top and left of the matrices indicates age groups (e.g., 2 represents age group $5-9$ and 16 represents age group 75+). The last column shows aggregated contact matrices considering all interaction settings.

groups).

Impact of vaccines and NPIs

Timing of vaccination impact

In the context of the no-vaccination counterfactual with the baseline model, we investigate when vaccinations start to have a macroscopic impact. To this end, we compute the time when the weekly deaths with/without vaccinations begin to diverge by at least 1% (i.e., the weekly relative difference of deaths exceeds this threshold). The results are shown in Fig. 8. The grey lines mark the start of vaccinations, and the red lines denote the week in which the vaccination begins to have impact. We find that the vaccination impact started 8 weeks after the first rollout in London. This is much earlier than that in British Columbia, Lombardy, and São Paulo, in which the vaccination impact started respectively 12, 10, and 10 weeks after the first rollout. The difference is likely due to the faster and earlier vaccine rollout in London with respect to the other regions. In addition, the confidence interval of weekly RDD values falls below 0, particularly in British Columbia. This phenomenon may be influenced by overlaps in the trajectories with and without vaccination in certain samples, as well as the stochastic effects in the simulations.

medRxiv preprint doi: https://doi.org/10.1101/2024.11.07.24316893; this version posted November 7, 2024. The copyright holder for this preprint (which was not certified by peer review) is the author/funder, who has granted medRxiv a license to display the preprint in perpetuity.
It is made available under a CC-BY-NC 4.0 International license .

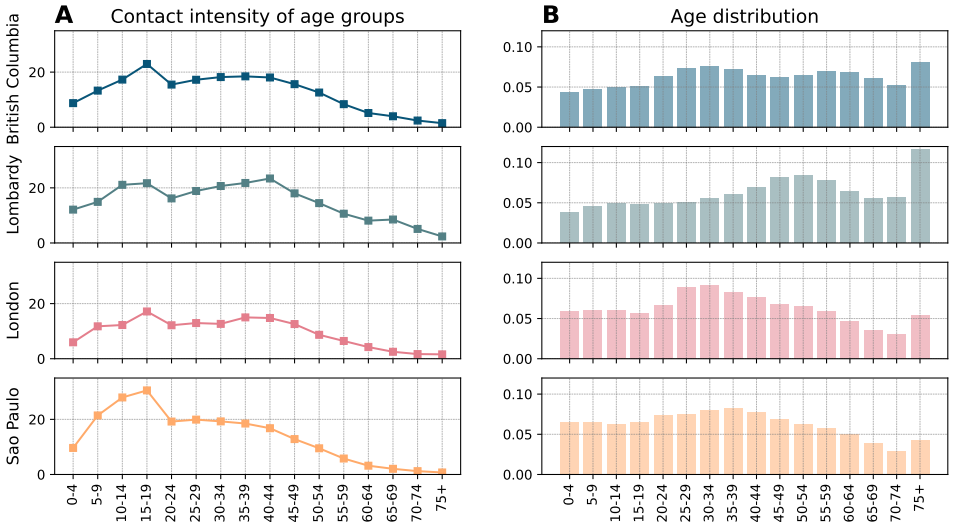

Fig 7. Contact intensity and demographics. A) Contact intensity across age groups in the four regions. Contact intensity is computed by summing each column of the contact matrix. B) Age distributions across the four regions with a 5-year bracket except for the last 75+ group.

Influence of NPIs on peak deaths

We analyze the impact of non-pharmaceutical interventions (NPIs) on deaths peak by calculating the fold increase in the peak intensity in a scenario without NPIs compared to the original model with NPIs. In doing so, we maintain vaccination in both scenarios. We first show the death trajectories with/without NPIs in Fig. 9. The peak of deaths without NPIs (red lines) is much higher than with NPIs (blue lines). The peak without NPIs also comes earlier (in terms of the median trajectory) compared to those with NPIs in London (3 weeks earlier) and São Paulo (2 weeks earlier). Next we show the fold increase in peak deaths in Fig. 10. Removing NPIs would have resulted in 5.8 (90% CI: $[2.9, 11.9]$) in British Columbia, 2.8 ($[1.9, 4.6]$) in Lombardy, 6.1 ($[5.0, 7.6]$) in London, and 4.6 ($[3.8, 5.7]$) in São Paulo times higher peaks. London reports the highest fold in peak deaths as it reports the most stringent NPIs compared to the other three regions. São Paulo reports higher increase compared to Lombardy despite the lower adoption of NPIs among the four regions. This may be due to demographic and social factors. Indeed, São Paulo has a larger proportion of young people with active social contacts.

Relative difference of infection in counterfactual scenarios without vaccination or NPIs

In the main text, we presented the relative deaths difference (i.e., RDD) with/without vaccination, NPIs, and behavioural relaxation. Here, we show the analogous results for the relative difference in the number of infected (i.e., RDI). This quantity is defined as:

$$RDI = \frac{I_{counterfactual} - I_{original}}{I_{counterfactual}} \times 100\% \tag{50}$$

where $I_{original}$ and $I_{counterfactual}$ are the total number of simulated infections in the original model

medRxiv preprint doi: https://doi.org/10.1101/2024.11.07.24316893; this version posted November 7, 2024. The copyright holder for this preprint (which was not certified by peer review) is the author/funder, who has granted medRxiv a license to display the preprint in perpetuity.
It is made available under a CC-BY-NC 4.0 International license .

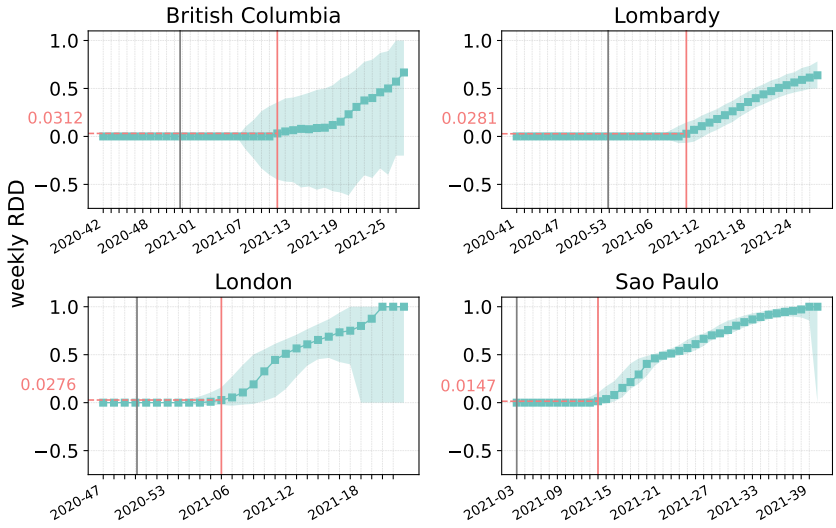

Fig 8. Weekly relative deaths difference in counterfactual scenarios without vaccinations. The fraction of deaths averted by vaccination each week with respect to an equivalent model without vaccinations. The grey lines mark the start of vaccinations while the red lines mark the week in which the relative difference of deaths is larger than 0.01 (0.0312 in British Columbia, 0.0281 in Lombardy, 0.0276 in London, 0.0147 in São Paulo). We show the results considering 1000 stochastic trajectories, median and 90% confidence interval.

and in the counterfactual scenario respectively.

For example, in the case of NPIs $I_{counterfactual}$ is computed considering estimates from a model without them. Instead, $I_{original}$ is the corresponding value in matched model with NPIs.

The RDIs in a scenario without vaccination are shown in Fig. 11-A. We compute the median of RDI with a 90% confidence interval considering 1000 stochastic trajectories. The results indicate that vaccination prevented 3.41% (90% CI: $[-0.25\%, 8.95\%]$) of infections in British Columbia, 12.96% ($[8.9\%, 17.6\%]$) in Lombardy, 2.42% ($[0.5\%, 5.6\%]$) in London, and 8.99% ($[6.84\%, 13.87\%]$) in São Paulo. The figures are generally smaller than RDDs (shown in the main text) across the four regions, since vaccines are more effective at preventing deaths than infections. Furthermore, the RDI rankings among British Columbia, Lombardy, and London exhibit a similar pattern to that observed for the RDD. However, São Paulo shows different pattern of RDI compared to RDD. Indeed, São Paulo has the largest vaccine coverage among the regions and it shows the highest RDD. However, it features a lower RDIs compared to RDDs. São Paulo experienced the Gamma and Delta variants, which reduce the vaccine efficacy against infections significantly. Also, as discussed above, São Paulo has a larger portion of younger individuals aged $10-19$ who are very socially active, resulting in a greater burden in terms of infections.

The RDIs of a counterfactual scenario without NPIs are shown in Fig. 11-B. We find 85.57% (90% CI: $[80.86\%, 89.44\%]$) infections avoided by NPIs in British Columbia, 49.65% ($[41.05\%, 57.42\%]$) in Lombardy, 44.91% ($[39.48\%, 50.12\%]$) in London, and 3.43% ($[-3.98\%, 12.56\%]$) in São Paulo. The RDIs of the four regions show similar patterns to the observations for RDDs. By comparing panel A and panel B in Fig. 11, we can conclude that overall, in the first months of vaccines rollout, NPIs averted

medRxiv preprint doi: https://doi.org/10.1101/2024.11.07.24316893; this version posted November 7, 2024. The copyright holder for this preprint (which was not certified by peer review) is the author/funder, who has granted medRxiv a license to display the preprint in perpetuity.
It is made available under a CC-BY-NC 4.0 International license .

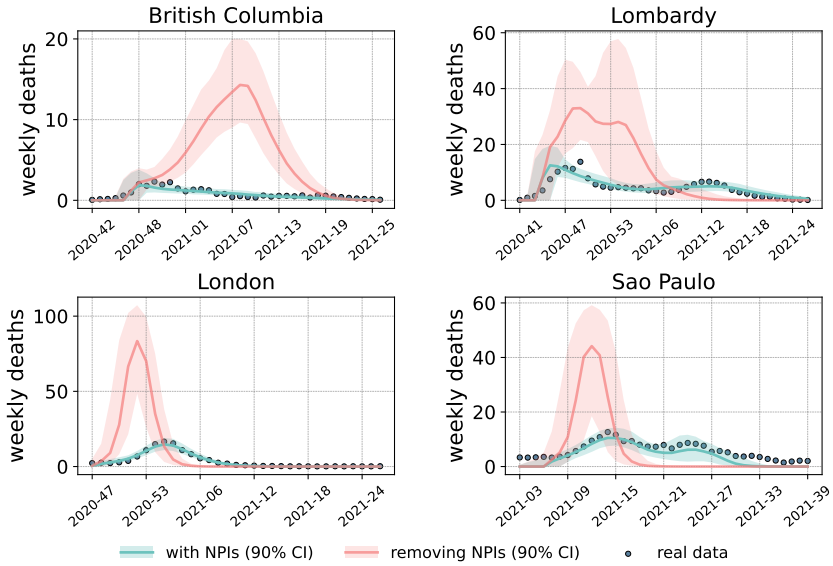

Fig 9. Comparison of weekly death trajectories with/without NPIs. Calibrated weekly death trajectories (weekly deaths per $100,000$) of the baseline model (denoted by blue lines) and in a counterfactual scenario where NPIs are removed (denoted by red lines).

more infections compared to those prevented by vaccinations. These results highlight one more time the importance of NPIs during the complex initial phases of the vaccination campaign.

Relative difference of infection in counterfactual scenarios without behavioural relaxation

We also calculate the relative difference of infections (RDIs) considering a counterfactual scenario where we remove the relaxation from the four behavioural models. The results are shown in Fig. 12 and Table 5, displaying the median of RDIs along with 90% CIs. The values of RDI are below 0 in most cases, which means removing behavioural mechanisms leads to fewer infections (see Table 5). Furthermore, the results for RDIs are consistent with the analogous for RDDs shown in the main text.

Table 5. Relative infection difference in counterfactual scenarios without behavioural relaxation.

RDI (%)	model 1	model 2	model 3	model 4
British Columbia	-1.90 [-34.27,2.9]	-1.05 [-19.57,2.71]	0.03 [-3.82,3.33]	-0.06 [-2.81,2.93]
Lombardy	-35.62 [-68.53,-2.16]	-0.35 [-9.94,0.58]	-0.30 [-1.77,0.58]	-0.08 [-0.9,0.6]
London	-0.99 [-29.81,0.1]	-0.14 [-4.48,0.19]	-0.06 [-0.44,0.2]	-0.01 [-0.28,0.22]
São Paulo	-0.15 [-9.76,0.37]	-4.29 [-30.32,0.07]	-0.69 [-3.7,0.12]	-0.19 [-2.76,0.19]

Absolute death differences across counterfactual scenarios

In the main text, we showed the relative deaths difference considering counterfactual scenarios without vaccinations, NPIs, or behavioural relaxation. Here, we show absolute values. We show the medians with 90% confidence interval in Tables 6-8.

As is shown in Table 6, the absolute deaths difference in counterfactual scenarios without vaccination is small in British Columbia with a median of 52 more deaths without vaccinations. In contrast, São Paulo shows a large difference with a median of more than $60K$.

medRxiv preprint doi: https://doi.org/10.1101/2024.11.07.24316893; this version posted November 7, 2024. The copyright holder for this preprint (which was not certified by peer review) is the author/funder, who has granted medRxiv a license to display the preprint in perpetuity.
It is made available under a CC-BY-NC 4.0 International license .

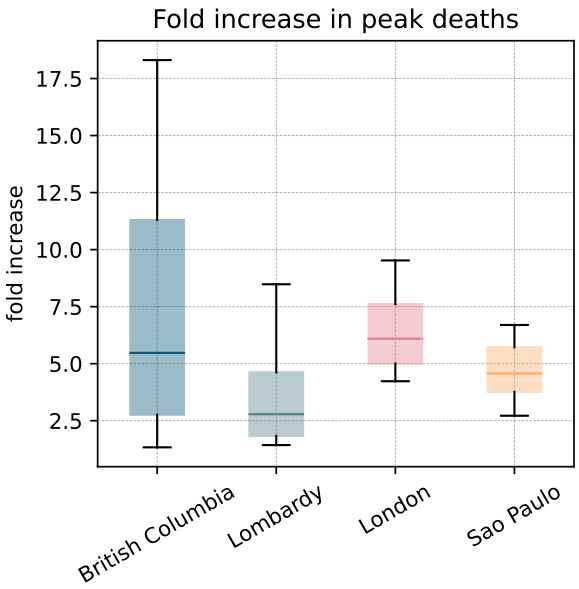

Fig 10. Fold increase in peak deaths intensity in counterfactual scenarios without NPIs. The increase fold of peak deaths in a scenario where NPIs are removed with respect to an equivalent case with NPIs. The box plots show the results of averted deaths considering 1000 stochastic trajectories in each region.

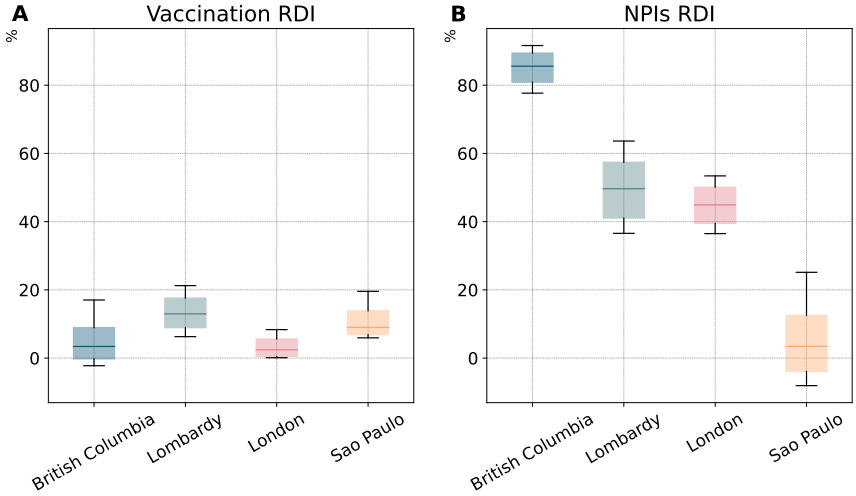

Fig 11. Relative infection difference in counterfactual scenarios without vaccinations and NPIs. Panel A shows the fraction of total infections averted by vaccinations. Panel B shows the fraction of total infections averted by NPIs. The box plots show the results of averted deaths in 1000 stochastic trajectories in each region.

The absolute deaths difference in counterfactual scenarios without NPIs is shown in in Table 7. The values are much higher than those of vaccination except a decrease in São Paulo. As mentioned in the main text, in São Paulo we observed the least stringent adoption of NPIs. These results underscore the importance of vaccinations, especially in settings with low adoption of NPIs.

In Table 8, we show the deaths difference in counterfactual scenarios without behavioural relaxation. Model 2, which as shown in the main text results as the most likely model in São Paulo, leads to highest number of deaths.

medRxiv preprint doi: https://doi.org/10.1101/2024.11.07.24316893; this version posted November 7, 2024. The copyright holder for this preprint (which was not certified by peer review) is the author/funder, who has granted medRxiv a license to display the preprint in perpetuity.
It is made available under a CC-BY-NC 4.0 International license .

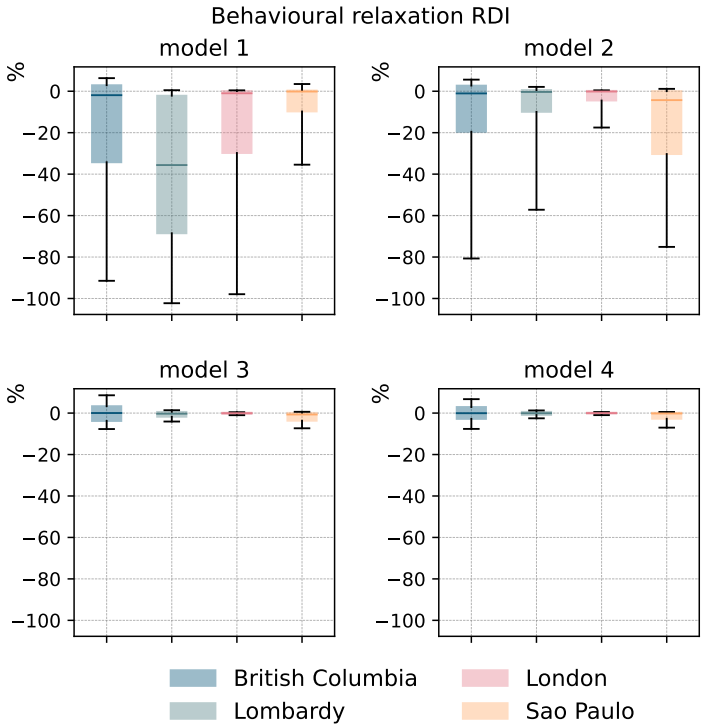

Fig 12. Relative infection difference in counterfactual scenarios without behavioural relaxation. The fraction of total infections averted by behavioural relaxation. The box plots show the results of averted deaths in 1000 stochastic trajectories in each region.

Table 6. Deaths difference in a counterfactual without vaccinations.

British Columbia	Lombardy	London	São Paulo
52 [-3,140]	2702 [1981,3318]	823 [168,2194]	64572 [52672,76191]

Impact of behavioural relaxation

Behavioural transition rate

In model 1 and 3 the transitions towards non-compliance and those back to compliance happen at constant rates, α and γ respectively. Instead, in models 2 and 4 these transitions are proportional to the fraction of vaccinated (multiplied by α) and deaths per $100,000$ (multiplied by γ). To better understand these varying transition rates, in Fig. 13-A we plot, for different values of α, the transition rates from compliant to non-compliant compartments as a function of the fraction of vaccinated individuals. We denote this rate as $h(\alpha, frac_V(t)) = 1 - e^{-\alpha frac_V(t)}$, where $frac_V(t)$ is the fraction of vaccinated individuals of the total population. Similarly, in Fig. 13-B we consider a range of γ values and plot the transition rates from compliant back to non-compliant as a function of daily new deaths per $100,000$ denoted by $h(\gamma, rate_D(t)) = 1 - e^{-\gamma rate_D(t)}$, where $rate_D(t)$ represents daily death rate (deaths per $100,000$).

The results in Fig. 13-A show that a higher fraction of vaccinated individuals leads to an increased

British Columbia	Lombardy	London	São Paulo
7774 [6157,9659]	23152 [16081,28069]	18922 [16309,22741]	36612 [26681,47563]

Table 7. Deaths difference in a counterfactual without NPIs

medRxiv preprint doi: https://doi.org/10.1101/2024.11.07.24316893; this version posted November 7, 2024. The copyright holder for this preprint (which was not certified by peer review) is the author/funder, who has granted medRxiv a license to display the preprint in perpetuity.
It is made available under a CC-BY-NC 4.0 International license .

Table 8. Death difference in a counterfactual without behavioural relaxation.

	model 1	model 2	model 3	model 4
British Columbia	-42 [-258,29]	-15 [-135,47]	-1 [-58,57]	0 [-47,51]
Lombardy	-4061 [-7028,-409]	-92 [-1553,182]	-67 [-354,192]	-18 [-256,202]
London	-140 [-2734,100]	-27 [-442,157]	-14 [-209,167]	-7 [-148,133]
São Paulo	-786 [-21572,379]	-5094 [-31443,345]	-765 [-3664,388]	-258 [-2783,459]

transition rates towards non-compliance. As α increases, the transition rate $h(\alpha, frac_V)$ rises more sharply. This means that, for a given fraction of vaccinated individuals, higher values of α result in a greater shift towards non-compliance. For example, when $\alpha = 0.1$, the transition rate is only 0.1 even when the fraction of vaccinated individuals reaches its maximum (1). In contrast, when $\alpha = 10$, the transition rate reaches 1 when only 40% of the population is vaccinated. A similar trend is observed in Fig. 13-B where higher daily death rates lead to higher transition rates from non-compliance back to compliance. Furthermore, higher values of γ result in stronger responses to the epidemic's severity. For example, when $\gamma = 0.1$, the transition rate is 0.2 even when the daily death rate is quite high (2). In contrast, when $\gamma = 10$, the transition rate reaches the maximum when the death rate is smaller (0.5).

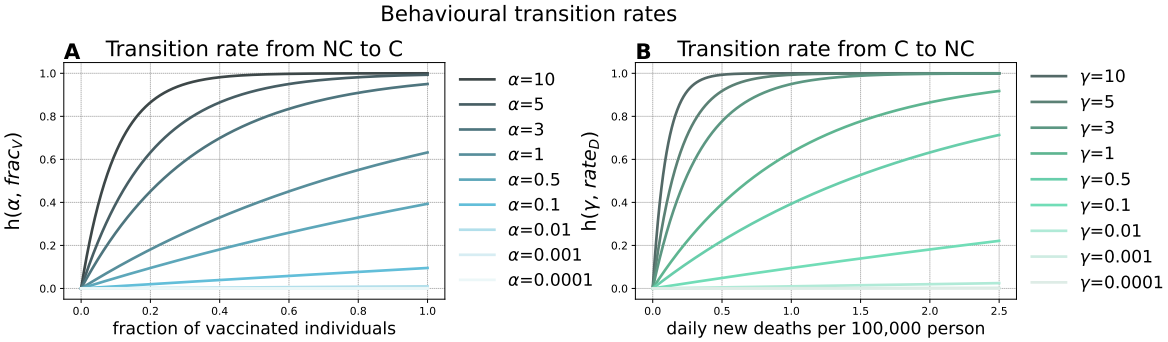

Fig 13. Behavioural transition rates for models 2 and 4. In panel A we plot the behavioural transition rate from non-compliant to compliant denoted by $h(\alpha, frac_V)$ as a function of the fraction of vaccinated individuals for different values of α. In panel B we plot the behavioural transition rate from compliant to non-compliant denoted by $h(\gamma, rate_D(t))$ as a function of the fraction of daily new deaths per $100,000$ for different values of γ.

Fraction of non-compliant individuals as function of time

To have a more intuitive understanding on the four behavioural mechanisms, in Fig. 14 we plot the fraction of non-compliant individuals as function of time for the four models. To this end, we consider 1000 simulations obtaining sampling the posterior distribution of each model. We then compute the fraction of non-compliant individuals for each. We show the median trajectory with 90% confidence intervals. Overall, we observe that model 1 and model 2 result in the largest fraction of non-compliant individuals, especially during the first time steps. We note also that the two models show the largest variability in terms of their confidence intervals. In the case of Lombardy, the median for model 1 quickly raises to about half of the population, a trend that is not observed in other locations. As shown below, this is consistent with the significative large values of α selected by the calibration for this model and

medRxiv preprint doi: https://doi.org/10.1101/2024.11.07.24316893; this version posted November 7, 2024. The copyright holder for this preprint (which was not certified by peer review) is the author/funder, who has granted medRxiv a license to display the preprint in perpetuity.
It is made available under a CC-BY-NC 4.0 International license .

location.

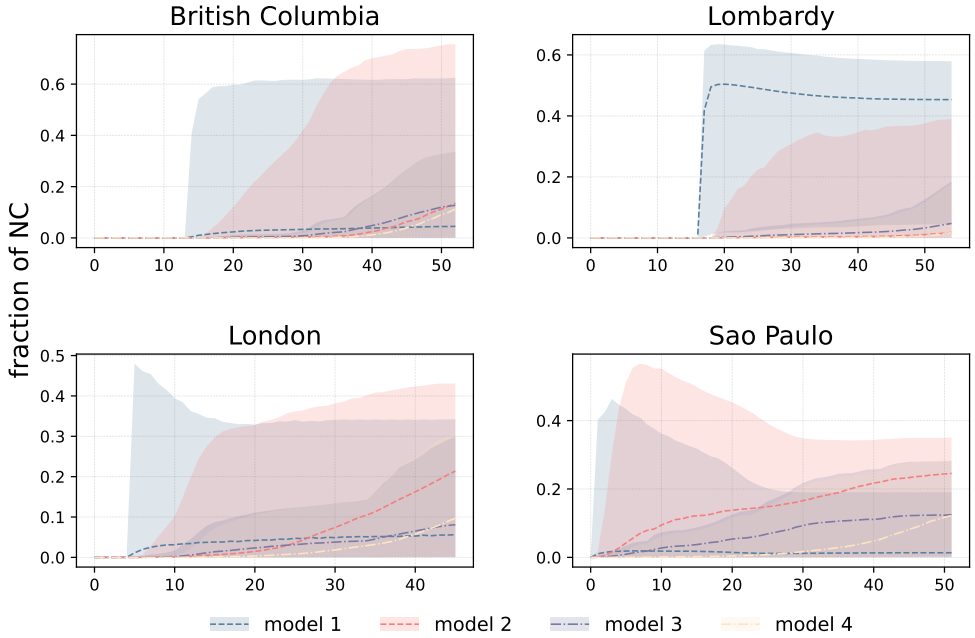

Fig 14. Fraction of non-compliant individuals as function of time. We plot the fraction of non-compliant individuals of the four behavioural models (models 1–4) in each region. The fractions are computed considering 1000 sampled trajectories. The dotted lines represent the median fractions, with shaded areas indicating the 90% confidence intervals.

Model calibration

AIC scores of models

In Table 9 we report the AIC scores of the five models. Smallest scores indicates a better performance of a model. As is shown, the baseline reports the smallest scores in the three regions (British Columbia, Lombardy, and London) out of four, while only one behavioural model (model 2) reports the smallest AIC score in São Paulo.

Table 9. AIC weights of models.

	baseline	model 1	model 2	model 3	model 4
British Columbia	**263.7**	269.1	269.5	269.9	269.9
Lombardy	**425.4**	436.7	431.1	432.3	434.4
London	**331.6**	338.8	336.5	337.9	338.7
São Paulo	501.9	511.3	**501.2**	506.0	505.8

Posterior distributions of parameters

In this section, we present the posterior distributions of the free parameters in our models computed via the Approximate Bayesian Computation-Sequential Monte Carlo (ABC-SMC). For each region, we plot the median values of the sampled parameters, along with the interquartile range (IQR) spanning from the first to the third quartile. Notably, the number of free parameters in the baseline model differs

medRxiv preprint doi: https://doi.org/10.1101/2024.11.07.24316893; this version posted November 7, 2024. The copyright holder for this preprint (which was not certified by peer review) is the author/funder, who has granted medRxiv a license to display the preprint in perpetuity.
It is made available under a CC-BY-NC 4.0 International license .

among regions due to the emergence of the second variant. Specifically, for the baseline model, in British Columbia and Lombardy, there are six free parameters to be calibrated: the reproductive number R_0, the delay time in reporting deaths Δ, the initial fraction of infected individuals i_{ini}, the initial fraction of recovered individuals r_{ini}, the adjustment of the start date of the simulation of epidemic Δt, and the adjustment of the introduction date of a VOC Δt_{var}. For London we have five free parameters as above, excluding Δt_{var}, as London experienced only one strain during the simulation period. In São Paulo, seven parameters are calibrated, the above six, as for British Columbia and Lombardy, and additionally the relative transmissibility (σ) of the Delta variant compared to the Gamma variant. As mentioned in the main text, this relative transmissibility for Alpha is fixed at 1.5 for British Columbia and Lombardy. Across all regions, the behavioural models (Models 1-4) consistently incorporate three additional behavioural parameters: the behavioural transition parameters α and γ, as well as the relative infection probability r of non-compliant individuals.

The posterior distributions of the four regions are shown in Figs. 15-18. We compare the posteriors across the regions. For the reproductive number R_0, the calibrated values span from 1.0 to 2.5. London exhibits the highest R_0 across all models, due to the circulation is Alpha variant at the beginning time of our simulations. British Columbia instead reports the lowest R_0, corresponding to the lowest observed epidemic burden among the four regions. The delay in reporting deaths (Δ) ranges from 43 to 64 days in British Columbia, Lombardy, and São Paulo in terms of the baseline model, whereas London shows a shorter delay of approximately 20 days. This difference may be due to difference in healthcare reporting systems. Regarding the posteriors of initial fraction of infected individuals i_{ini}, Lombardy stands out with the fraction above 0.007 while the other three regions show a value below this. The posteriors of the fraction of recovered r_{ini} show the highest value in Lombardy. This is consistent with the fact that Lombardy experienced the highest mortality rate across the four regions till the start date in our simulation. The adjustment of the start date of simulations (Δt) are in the range of $2-6$ weeks across the regions, which indicates that the start dates are $2-6$ weeks before the baseline date (t^*). The adjustment of the introduction date of a VOC Δ_{var} is in the range of 14-28 days in British Columbia and São Paulo, and 0-14 days in Lombardy except model 1 reports the range 14-28 days.

In terms of the parameters in the behavioural models, the values of α and γ are both relatively small in British Columbia across the four behavioural models than the other three regions. The relative infection probability r of non-compliant individuals are similar across the regions in the range between 1.1 and 1.4.

medRxiv preprint doi: https://doi.org/10.1101/2024.11.07.24316893; this version posted November 7, 2024. The copyright holder for this preprint (which was not certified by peer review) is the author/funder, who has granted medRxiv a license to display the preprint in perpetuity.
It is made available under a CC-BY-NC 4.0 International license .

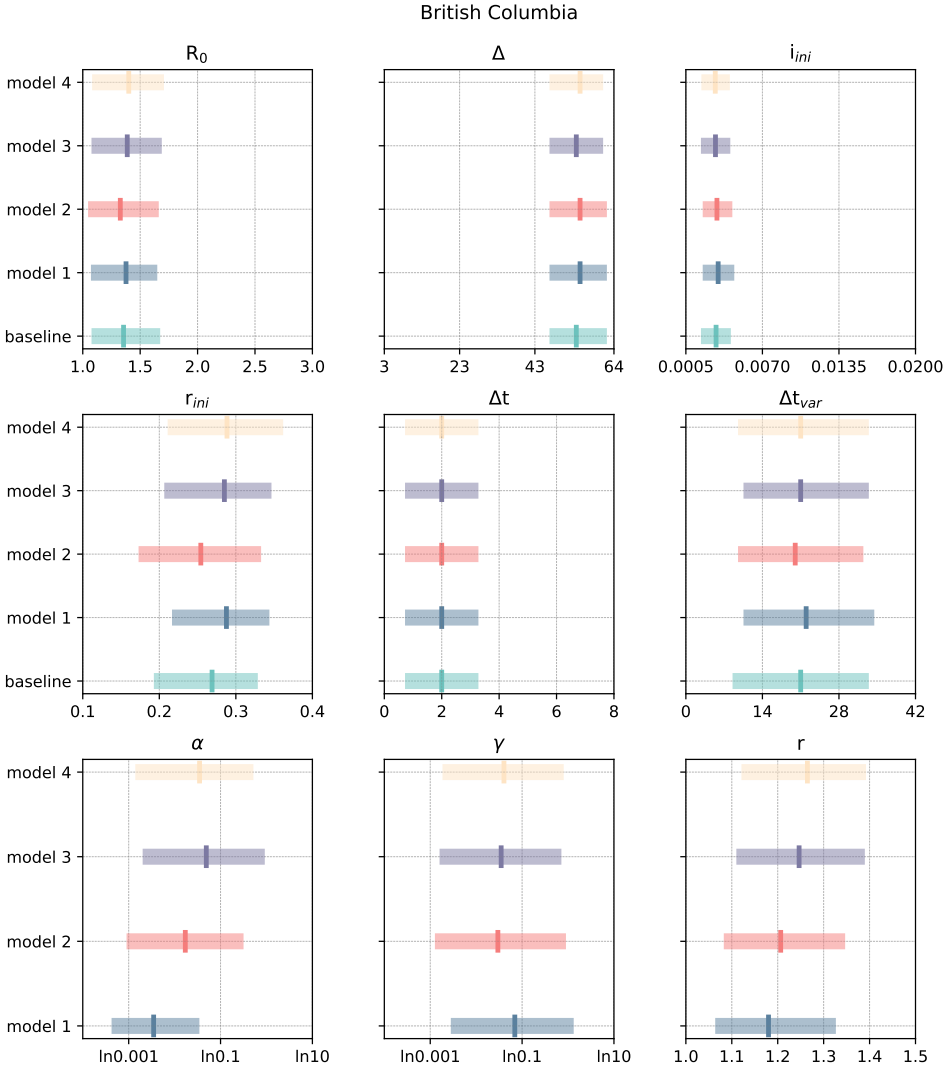

Fig 15. Posterior distributions of calibrated parameters for British Columbia. We plot the median with the range between first quartile and third quartile. The first sixth parameters, R_0, Δ, i_{ini}, r_{ini}, Δt, Δt_{var} are calibrated in all the five models. α, β, and r are behavioural parameters only in behavioural models (models 1-4).

medRxiv preprint doi: https://doi.org/10.1101/2024.11.07.24316893; this version posted November 7, 2024. The copyright holder for this preprint (which was not certified by peer review) is the author/funder, who has granted medRxiv a license to display the preprint in perpetuity.
It is made available under a CC-BY-NC 4.0 International license .

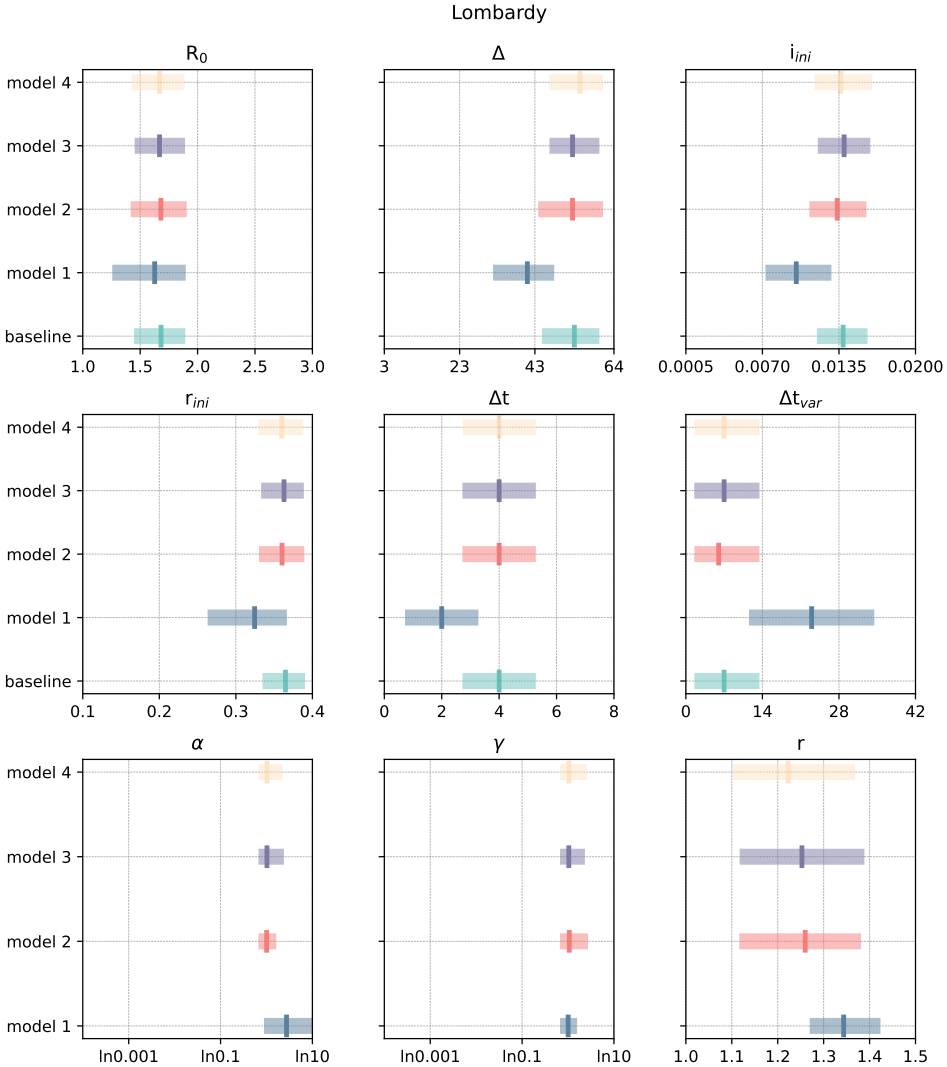

Fig 16. Posterior distributions of calibrated parameters for Lombardy. We plot the median with the range between the first quartile and the third quartile. The first sixth parameters, R_0, Δ, i_{ini}, r_{ini}, Δt, Δt_{var} are calibrated in all the five models. α, β, and r are behavioural parameters only in behavioural models (models 1-4).

medRxiv preprint doi: https://doi.org/10.1101/2024.11.07.24316893; this version posted November 7, 2024. The copyright holder for this preprint (which was not certified by peer review) is the author/funder, who has granted medRxiv a license to display the preprint in perpetuity.
It is made available under a CC-BY-NC 4.0 International license .

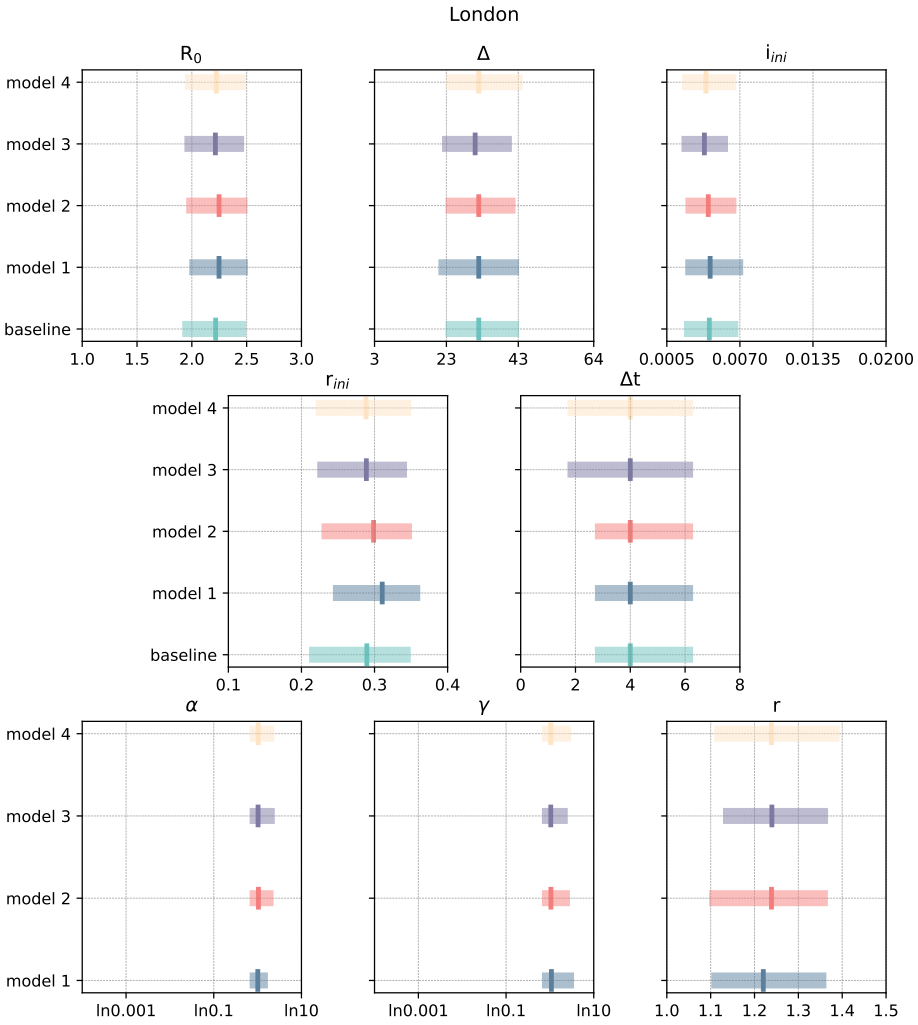

Fig 17. Posterior distributions of calibrated parameters for London. We plot the median with the range between the first quartile and the third quartile. The first sixth parameters, R_0, Δ, i_{ini}, r_{ini}, Δt are calibrated in all the five models. α, β, and r are behavioural parameters only in behavioural models (models 1-4).

medRxiv preprint doi: https://doi.org/10.1101/2024.11.07.24316893; this version posted November 7, 2024. The copyright holder for this preprint (which was not certified by peer review) is the author/funder, who has granted medRxiv a license to display the preprint in perpetuity.
It is made available under a CC-BY-NC 4.0 International license .

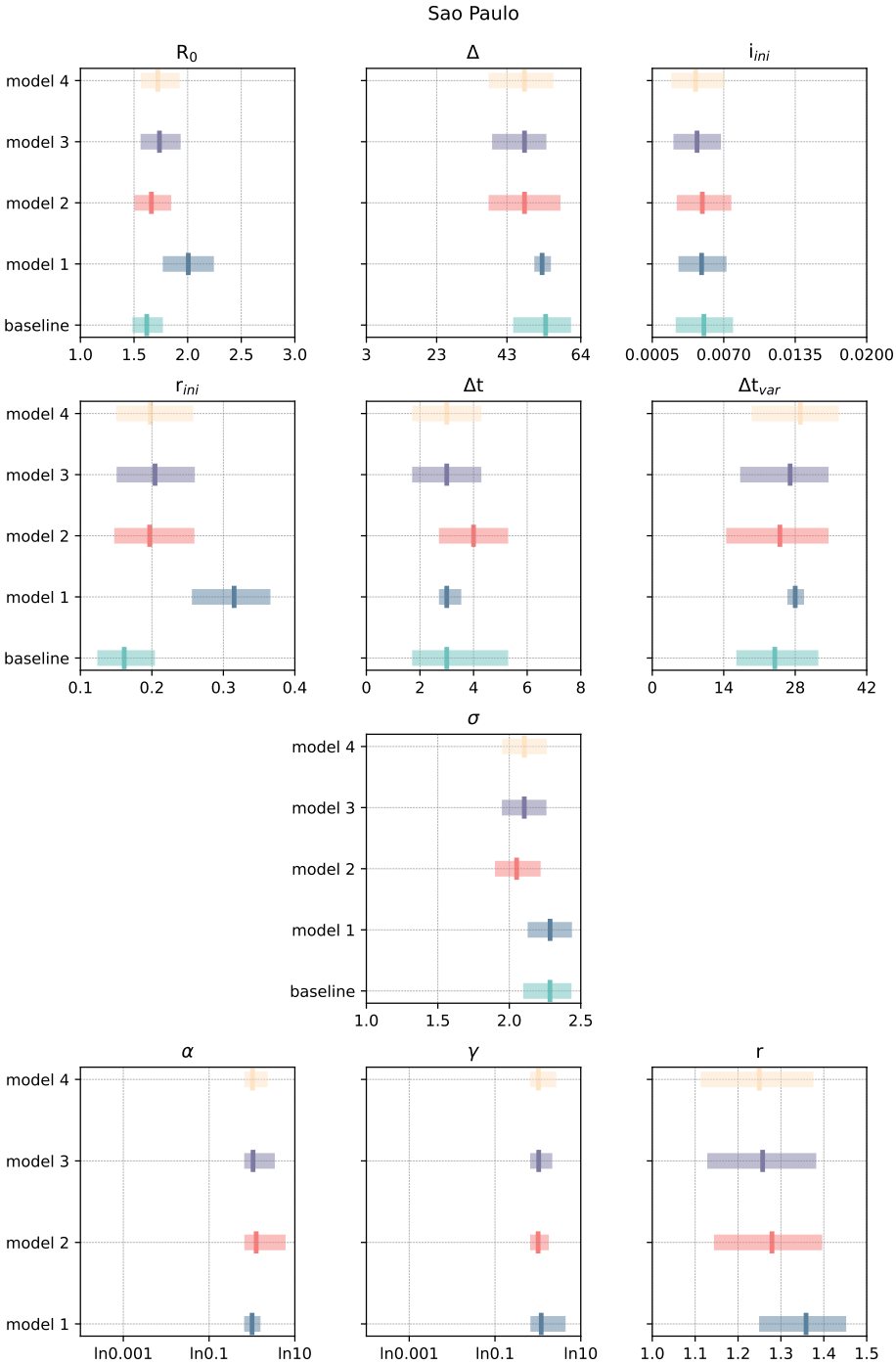

Fig 18. Posterior distributions of calibrated parameters for São Paulo. We plot the median with the range between the first quartile and third quartile. The first sixth parameters, R_0, Δ, i_{ini}, r_{ini}, Δt, Δt_{var}, σ are calibrated in all the five models. α, β, and r are behavioural parameters only in behavioural models (models 1-4).